Mälardalen University Press Dissertations
No. 157

MEASUREMENT SYSTEM FOR MICROWAVE IMAGING TOWARDS A BIOMEDICAL APPLICATION

Nikola Petrović

2014

School of Innovation, Design and Engineering

ISBN 978-91-7485-146-5
ISSN 1651-4238
Printed by Arkitektkopia, Västerås, Sweden

Mälardalen University Press Dissertations
No. 157

MEASUREMENT SYSTEM FOR MICROWAVE IMAGING TOWARDS A BIOMEDICAL APPLICATION

Nikola Petrović

Akademisk avhandling

som för avläggande av teknologie doktorsexamen i elektronik vid Akademin för innovation, design och teknik kommer att offentligen försvaras onsdagen den 28 maj 2014, 10.00 i Paros, Mälardalens högskola, Västerås.

Fakultetsopponent: Professor Christian Pichot, University of Nice

Akademin för innovation, design och teknik

Abstract

Microwave imaging techniques have shown excellent capabilities in various fields such as civil engineering, nondestructive testing, industrial applications, and have in recent decades experienced strong growth as a research topic in biomedical diagnostics. Many research groups throughout the world work on prototype systems for producing images of human tissues in different biomedical applications, particularly breast tumor detection. However, the research community faces many challenges and in order to be competitive to other imaging modalities one of the means is to put emphasis on experimental work. Consequently, the use of flexible and accurate measurement systems, together with the design and fabrication of suitable antennas, are essential to the development of efficient microwave imaging systems.

The first part of this thesis focuses on measurement systems for microwave imaging in terms of antenna design and development, robot controlled synthetic array geometries, permittivity measurements, and calibration. The aim was to investigate the feasibility of a flexible system for measuring the fields around an inhomogeneous object and to create quantitative images. Hence, such an aim requires solving of a nonlinear inverse scattering problem, which in turn requires accurate measurements for producing good quality experimental data. The presented solution by design of a flexible measurement system is validated by examination of microwave imaging from experimental data with a breast phantom.

The second part of the thesis deals with the research challenges of designing high performance antennas to be placed in direct contact with or in close proximity to the imaged object. The need for novel antenna applicators is envisaged in the framework of the Mamacell measurement system, where the antenna applicators have to be designed and constructed to effectively couple the energy into the imaging object. For this purpose the main constraints and design requirements are a narrow lobe of the antenna, very small near-field effects, and small size. Numerical simulations and modeling shows that the proposed ridged waveguide antenna is capable of fulfilling the design requirements and the performance goals, demonstrating the potential for the future microwave imaging system called Mamacell.

ISBN 978-91-7485-146-5
ISSN 1651-4238

In loving memory of my brother Ljubiša

Abstract

Microwave imaging techniques have shown excellent capabilities in various fields such as civil engineering, nondestructive testing, industrial applications, and have in recent decades experienced strong growth as a research topic in biomedical diagnostics. Many research groups throughout the world work on prototype systems for producing images of human tissues in different biomedical applications, particularly breast tumor detection. However, the research community faces many challenges and in order to be competitive to other imaging modalities one of the means is to put emphasis on experimental work. Consequently, the use of flexible and accurate measurement systems, together with the design and fabrication of suitable antennas, are essential to the development of efficient microwave imaging systems.

The first part of this thesis focuses on measurement systems for microwave imaging in terms of antenna design and development, robot controlled synthetic antenna array geometries, permittivity measurements, and calibration. The aim was to investigate the feasibility of a flexible system for measuring the fields around an inhomogeneous object and to create quantitative images. Hence, such an aim requires solving of a nonlinear inverse scattering problem, which in turn requires accurate measurements for producing good quality experimental data. The presented solution by design of a flexible measurement system is validated by examination of microwave imaging from experimental data with a breast phantom.

The second part of the thesis deals with the research challenges of designing high performance antennas to be placed in direct contact with or in close proximity to the imaged object. The need for novel antenna applicators is envisaged in the framework of the Mamacell measurement system, where the antenna applicators have to be designed and constructed to effectively couple the energy into the imaging object. For this purpose the main constraints and design requirements are a narrow lobe of the antenna, very small near-field effects, and small size. Numerical simulations and modeling shows that the proposed ridged waveguide antenna is capable of fulfilling the design requirements and the performance goals, demonstrating the potential for the future microwave imaging system called Mamacell.

Sammandrag

Mikrovågsavbildningstekniker har påvisat utmärkta möjligheter inom olika områden såsom anläggningsarbeten, oförstörande provning, industriella tillämpningar, och har under de senaste decennierna haft en stark tillväxt som ett forskningsämne inom biomedicinsk diagnostik. Många forskargrupper runt om i världen jobbar på prototypsystem för att framställa bilder av mänsklig vävnad i olika biomedicinska tillämpningar, särskilt för brösttumördetektion. Dock står forskarvärlden inför många utmaningar och för att vara konkurrenskraftiga bland andra avbildningsmetoder så är ett av medlen att lägga tonvikten på experimentellt arbete. Följaktligen är användningen av flexibla och noggranna mätsystem, tillsammans med design och tillverkning av lämpliga antenner, avgörande för utveckling av effektiva mikrovågsavbildningssystem.

Den första delen av avhandlingen fokuserar på mätsystem för mikrovågsavbildning i form av design och utveckling av antenner, robotgenererande syntetiska antenngeometrier, permittivitetsmätningar och kalibrering. Syftet var att undersöka möjligheten att med ett flexibelt system mäta fälten runt ett inhomogent objekt och att skapa kvantitativa bilder av objektets inre. Med detta mål i sikte krävs en lösning i form av ett icke-linjärt inverst spridningsproblem, vilket i sin tur kräver noggranna mätningar för att producera högkvalitativ experimentell data. Den presenterade lösningen, genom utformningen av ett system för flexibla mätningar, validerades genom undersökning av mikrovågsavbildning från experimentella data med en bröstfantom.

Den andra delen av avhandlingen behandlar forskningsutmaningar för design av högprestanda-antenner som placeras i direkt kontakt med, eller i nära anslutning till det avbildade objektet. Behovet av nya antennapplikatorer planeras inom ramen för mätsystemet Mamacell, där antennapplikatorer måste konstrueras och tillverkas för att effektivt koppla energi in i avbildningsobjektet. För detta ändamål är de huvudsakliga begränsningar och konstruktionskrav en smal antennlob, mycket små närfälts-effekter, och liten storlek. Numeriska simuleringar och modellering visar att den föreslagna vågledarantennen uppfyller design- och prestandakraven, vilket visar potentialen för det framtida mikrovågsavbildningssystem Mamacell.

Acknowledgements

Finally, a long, stimulating, educating, and challenging journey has come to an end, and just with a couple of hours left to finish the manuscript for printing, I am reflecting over the years as a PhD student. By closing my eyes, and trying to remember all the people I've met on this journey brings up nice memories. I am truly grateful for having had the chance of meeting and working with all of these competent and exciting people, of which I am very proud.

It has been a road with many ups and downs and in those moments it's very important to have a team of people around you that obviously care about you and wants you to do well, and I feel that I've had all that in place. I would like to express my deepest thanks to my supervisors, starting with my former supervisor Denny Åberg, thank you for taking me on as a PhD student in the first place and for introducing me to the exciting worlds of microwaves. My next supervisor and friend Magnus Otterskog, you have always been there for me encouraging, supporting and finding solutions to problems, I appreciate your way of always being a calm and nice person. My supervisor Mikael Ekström, thank you for your advices and for the positive way of thinking, which infected the writing of this thesis. Last but not least, I want to thank my supervisor Tommy Henriksson. You have not only been my colleague and supervisor, but also a great friend always been there and guided me many times. I wish you all the best in the future, and I am sure that we will keep in touch! I am also very grateful to Maria Lindén for always supporting and believing in me and our project.

I would also like to thank some of our professors at MDH for the great PhD courses; Hans Hansson, Gordana Dodig-Crnković and Jan Gustafsson. Thanks to professor Mats Björkman for reviewing my PhD proposal.

Special thanks to Per Olov Risman, with whom I worked for the last year. Thank you for all the interesting talks and writing the last paper together, you have in every situation respond to my questions and worked fast. I admire your way of solving problems and hope we can continue with the fruitful collaboration in the future. I am thankful to Nadine Joachimowicz and Alain Joisel for welcoming me for a visit at L2S/Supélec, and for the valuable discussions and advice. Thanks to Tiago Silva who was working with me at the beginning of my journey. I would like thank Robotdalen and specially Ingemar Reyier for the loan

and support with the industrial robot. Also, thanks to Jürgen Nolte at Västerås Finmekaniska for support in fabricating the antenna applicator.

It was a pleasure meeting all the nice people at the conference trips, especially the friendly people from Canada Jeremie Bourqui and Jeff Sill. Thanks Jeremie for answering to our emails.

I thank professor Christian Pichot for taking the time and coming to Västerås to act as opponent for this thesis and also the grading committee for the involvement in the dissertation.

I have enjoyed the stimulating and friendly working atmosphere at IDT — thanks to everyone! Special thanks to all my colleagues whom I have had the pleasure to share an office with and for all the interesting discussions during coffee breaks and lunches; Martin, Jimmie, Marcus, Gregory and Christer. Thanks to my friends and colleagues Aneta and Juraj, it's always nice to meet you and socialize. I would also like to thank my other close colleagues for making my time pleasant during breaks, lunches and IFT trips; Fredrik E., Carl, Mirko, Giacomo, Malin Å., Anna Å., Lars A., JF, Miguel, Radu, Andreas G., Luka, Josip, Zdravko, Leo, Federico, Aida, Adnan, Hüseyin, Moris, Mikael Å., Farhang, Rafia, Jagadish, Abhilash, Yue, Batu, Stefan B., Per H., Mattias O., and all others at IDT the list is long. In addition, I would like to thank Ingrid, Carola, Jenny, Anna, Susanne, Malin S., Sofia, Therese, Malin R., and Gunnar for taking care of administrative issues.

I would also like to give a big thanks to my great friend Johannes Kron. With whom I studied from the first day at MDH, thank you for all the nice study times and for sharing your knowledge with me.

Thanks to all my friends and relatives in Sweden, Serbia and Florida, you are too many to mention in this thesis, but you have all contributed a lot to my life, and I love spending my time with you.

No doubt my family is my driving force, and without them this would not have been possible. My parents Mirjana and Svetozar, thank you from all my heart for the unconditional love, understanding and support in every way. Thanks to my aunt Nada and my cousin Nataša, even though thousands of kilometres away, you have given me positive energy. My dear wife Ivana, and my children David, Marija and Jovana you are the most beautiful I have been given in life and I love you with all my soul, and your love is my inspiration. At last, thanks to my heavenly Father for all the strength and hope you have given me.

Nikola Petrović, Västerås, April, 2014

List of Publications

The following is a list of publications that form the basis of the thesis:

Paper A

Robot Controlled Data Acquisition System for Microwave Imaging
Nikola Petrović, Tommy Gunnarsson, Nadine Joachimowicz, and Magnus Otterskog
3rd European Conference on Antennas and Propagation (EuCAP 2009), pp.3356-3360, VDE Verlag GMBH, Berlin, March 2009

Paper B

Permittivity Measurements with a Resonant Cavity to Develop Human Tissue Phantoms for Microwave Imaging
Nikola Petrović and Magnus Otterskog
The 8th International Conference on Electromagnetic Wave Interaction with Water and Moist Substances, ISEMA 2009, Helsinki, Finland, June 2009

Paper C

Antenna Modeling Issues in Quantitative Image Reconstruction Using a Flexible Microwave Tomography System
Nikola Petrović, Tommy Henriksson, and Magnus Otterskog
PIERS Proceedings, pp. 952 - 956, July 5-8, Cambridge, USA 2010

Paper D

A Novel Flexible Data Acquisition System for Quantitative Microwave Imaging
Nikola Petrović, Tommy Henriksson, Mikael Ekström, and Magnus Otterskog
Submitted to IEEE Transactions on Instrumentation and Measurement, April 2014

Paper E

Antenna Applicator Design for Microwave Imaging of the Interior of Human Breasts
Nikola Petrović, Magnus Otterskog, and Per Olov Risman
Submitted to Journal of Physics D: Applied Physics, April 2014

Contents

Chapter 1

Introduction

This chapter introduces and describes the concept of microwave imaging with some applications in the biomedical field. Then following a summary of related research overview of experimental setups with highlight on the hardware design. Also, a short description of a clinical system is summarized. The remaining part of this section will discuss some of the image reconstruction algorithms, following the motivation with an emphasis on alternative techniques for breast imaging. The thesis organization will be described at the end of this Chapter.

1.1 Basic Concept of Microwave Imaging

The concept of using microwave frequency electromagnetic waves for imaging of dielectric bodies has extensively interested engineers and researchers for some decades. Microwaves refer to alternating current signals in the frequency range from 300 MHz to 300 GHz, which allow penetration into many optically not transparent mediums such as biological tissues, soil, wood, concrete, etc. Some of the applications that have been deployed for microwave imaging systems are ground penetrating radar, weapon detection, imaging through wall, and non-destructive testing for structural reliability.

Microwave imaging for biomedical applications is nowadays of very significant interest, having the potential of providing information about both physiological states and anatomical structures of human tissues.

The imaging with microwaves allows non-destructive evaluation of biological tissues due to the non-ionizing nature of microwaves, since changes in the dielectric properties of tissue can be related to their physiological condition. Several microwave imaging applications have been proposed in the biomedical field. One of the most promising application deployed is detection of breast tumors [1–4]. This is particularly eligible due to the easy approach of the breast for imaging, as well as the breast anatomy where the fatty tissue (with low loss) has a low attenuation impact on the signal. The contrast in permittivity for different in-vivo tissues (fat, glandular, malign tumour, vascular tissue etc.) is higher for microwaves than the most successful tool used today—X-ray Computed Tomography (CT)—is able to produce. For this reason, microwave imaging has been developed and has the potential to be a complementary modality to standard mammography. However it remains a field with many uncharted domains, and microwave imaging techniques need to overcome many challenges and be improved. This includes the enhancement of both more sophisticated hardware (antenna, electromechanical parts and RF-design) as well as in the software (imaging algorithms) to be considered as a reliable modality for biomedical application.

1.2 Related Work – Microwave Imaging Systems and Techniques

The emerging microwave imaging technique is a multidisciplinary area involving several research fields such as microwave engineering, electromagnetics, computer science, mathematics and clinical research. The joint work and advances in these areas have made the progress in microwave imaging techniques possible.

Microwave imaging systems for biomedical applications can roughly be divided into two main groups: active and passive systems. In passive systems, the radiation energy is received from the imaged object in the form of low level electromagnetic fields from warm human tissues [5]. The majority of the systems are active systems which mean that the illumination energy is generated by the measurement system. In this thesis, we focus on active systems and today there are two main approaches to active microwave imaging: microwave tomography [3, 6–11] and radar-based imaging [12–17]. In the former method the object is illuminated with microwaves and the scattered field is measured around

the object at a number of different positions. Multiple transmitter and receiver antennas can be used, or single transmitter or receiver configurations can illuminate the object and sample the scattered fields at multiple positions. Then by solving an inverse scattering problem the image of the object can be produced in terms of the spatial distribution of the complex permittivity. In the radar approach, the object is normally illuminated with short microwave pulses and the scattered response is received by one or several antennas. The image reconstructed from the measured scattering is based on the strong significant scatters of the imaged object and the most common algorithm in radar based systems is the confocal or delay-and-sum focusing algorithm.

1.2.1 Experimental Setups

Microwave imaging techniques and its application to medical imaging have attracted the interest of many research groups around the world since the first experiments with hardware systems in the late 1970s [18–20]. The pioneers, Larsen and Jacobi, developed a system where the transmission coefficient between two antennas, one transmitting and one receiving, was measured and images of the internal structure of a canine kidney was presented [18]. In their hardware setup, the antennas with the imaged object are immersed into a tank filled with water as a coupling liquid [19]. This arrangement is one of the fundamental approaches, even in many microwave imaging systems today, to effectively couple the microwave energy into the tissue. The results opened up for another hardware setup with the initial design and experiments of the planar microwave camera by researchers in Paris [20, 21]. This planar microwave system is constructed by two horn antennas, one transmitter and one receiver. In the front of the receiving antenna a matrix of 32x32=1024 sensors (dipole antennas) is used, a so called Modulated Scattering Technique (MST) [22], to enable quick data acquisition. This is quite an interesting hardware solution, because the sensors only use a frequency of 200 kHz and modulates the planar carrier wave frequency of 2.45 GHz. One of the applications with the planar microwave camera was to produce qualitative images of the temperature distributions of biological tissues to control the effect during hyperthermia treatment [23, 24]. The camera has been further developed since then to produce quantitative results [25], as well as qualitative results in a quasi real-time manner [26]. In the early 1990s the circular 2.45 GHz camera was de-

veloped with 64 antennas, which produced reconstructed images of a human forearm [27, 28]. The circular geometry of the receivers around the object was confirmed as a better choice for image reconstructions than the linear experimental geometry [27, 29]. Many research groups have followed this course thereafter and developed other experimental setups [30, 31].

One of the main potentials of microwave tomographic imaging is that it can provide quantitative information of the imaged object's dielectric properties, which makes it possible to identify tissues and materials. It has been shown that the microwave tissue dielectric properties are strongly dependent on physiological condition of the tissue [30], which plays a major roll to open opportunities for microwave imaging technology within medical diagnostics.

An experimental setup, of a microwave imaging prototype system developed by Semenov *et al.* utilize 64 waveguide antennas in a circular array, divided into 32 emitters and 32 receivers avoiding the isolation problems between the channels, operating at a frequency of 2.45 GHz [30]. With this system the group reconstructed a systolic and diastolic image of the beating canine heart and the total acquisition times was less than 500 ms. The antennas are located on the boundary of the cylindrical chamber filled with various solutions including distilled water. The waveguide antennas, operating in TE_{10} mode, are constructed with a three time wider field pattern in the horizontal plane compared to the vertical plane. This adjustment was done to try if it was possible to use a 2D diffraction model and create 2D images slicing a 3D object similar to the X-ray tomography technique. Their conclusion and suggestion where, to reconstruct a quantitative 3D object it is necessary to have a 3D system, so the "slice" technology used in X-ray tomography could not be used.

Meaney *et al.* developed a circular microwave imaging system, similar to Semenov *et al.*, for reconstruction of 2D electrical property distributions. In the first setup they also used waveguide's antennas (four) for transmitting, but monopole antennas (four) as receivers. The system operates at frequencies between 300 - 1100 MHz [31].

The Debye relaxation of water results in minimal penetration between 15 and 30 GHz, so one has to use either much lower or higher frequencies. However, other phenomena limit the microwave penetration at terahertz frequencies in tissues with high water content to some few millimetres. Today most of the microwave imaging systems work in a range between

0.5 to 10 GHz, where it is expected to have a good trade-off between the penetration depth and resolution.

Another system, for 3D microwave imaging, by Semenov *et al.* is built around a larger metallic chamber and with a network analyzer as a transceiver [32]. In this system only two waveguide antennas are used, both tuned to operate in salt solutions at a frequency range between 0.8 and 1 GHz. The waveguide antennas are set on two different arms, and with the use of a computer controlled robotic system they are positioned at various points inside the chamber while the object is fixed in the middle of the chamber. Both antennas can be rotated individually under the data acquisition, which makes it possible to measure the components (vertical and horizontal) of the electromagnetic field. The electromechanical part of the system requires high accuracy and stability because the data acquisition time is approximately 9 hours. These requirements are realized using accurate microwave and electronic components and optoelectronic control of mechanic position of antennas. However, there is still some instability in the technical parameters due to the long data acquisition time, but more critical is the physiological instability of the object and the coupling medium inside the chamber, which are the main reasons for the limited image quality. Another limitation of the image quality is the inadequacy in the mathematical model of the tomography experiment. Regardless of these limiting factors the group obtained images of a full size canine and that is an important milestone in the progress of microwave imaging.

Generally 3D microwave imaging is limited even today with the state-of-the-art hardware and most sophisticated algorithms, implemented on multiprocessors and GPU:s, the imaging reconstruction process time can take several hours. This is due to the full field computations for each antenna position.

Many other research groups have joined the biomedical microwave imaging field, especially the breast cancer detection [33–38]. Another upcoming biomedical application, to identify and categorize strokes effectively and quickly, has been presented in recent reports [39–41].

1.2.2 Clinical Systems for Microwave Breast Imaging

Experimental systems that can be used for clinical investigations of microwave breast imaging are not as many as the systems based on phantom

experiments. Meaney *et al.* were the first to develop a clinical prototype for active microwave imaging of the breast in the early 2000s [42]. The hardware has been designed to have each antenna operate in either transmit or receive mode. In this case, they used 16 monopole antennas in a circular array configuration, and a reason for using the monopole antennas is that the monopole can be effectively modelled as a line source in a 2D imaging problem. Another advantage is that, even if monopole antennas typically show undesirable characteristics when operating in a lossless medium (narrow bandwidth and excitation of surface waves), they are excellent radiators in a lossy environment where the usable bandwidth is increased with no evident excitation of surface currents. The purpose of this system is to detect early stage breast tumours with quantitative images. The system is based on their earlier work [43, 44] where they have mounted the system on a transportable bed with a hole for breast insertion. This study has been performed on real patients of different ages and breast images of five patients have been obtained. The initial results gave sliced 2D images of the human breast with a reasonable resolution. One important thing that the group is mentioning in this setup is to model each nonactive antenna as a microwave sink so the entering signals (E-field) are absorbed and not re-radiated. In the hardware, they have selected to use matched switches so when an antenna is in the nonactive state any coupled signal is transmitted through a coaxial cable into the switch with a matched termination without being re-radiated. Over the last decade many improvements have been done on the system both in algorithms and hardware [3, 45, 46]. So today one could say that this system is the state-of-the-art regarding microwave imaging for breast cancer detection. In addition to breast imaging the group have performed initial clinical trials for bone imaging using the same system [47, 48].

More recently Fear *et al.* performed a clinical trial of microwave breast imaging with a monostatic radar-based system [2]. Also a research group at the University of Bristol in U.K., have reported clinical tests of a multistatic radar approach [49].

1.2.3 Image Reconstruction Algorithms

Despite of all the possible advantages of microwave imaging, today only a few prototype systems are usable for real clinical investigations [2–4, 48, 50]. There are several difficulties that needs to be resolved. The

propagation of microwaves in comparison to X-rays are very complex and can not be easily modelled as a pencil beam propagation along a straight line of an X-ray. Due to this nature of microwaves the wide beam will create high scattering and diffraction of signals in the imaging object demanding more complicated computational heavy algorithms for obtaining an image from the measured data. Notable, in tomographic microwave imaging it is possible applying a more simple (computation efficient) linear approach using Born or Rytov approximations [20,27,51]. However, this approximation is only valid for weak scattering- and low-loss objects [52, 53]. The total field at each point inside the object must be equal to the incident field used for illumination with no object present. This fact limits the application towards biomedical ones. In [54] the authors concluded, that in the case of stronger scattering, it is necessary to assume nonlinear models.

One of the approaches in tomographic microwave imaging is nonlinear inverse scattering often referred to as nonlinear microwave tomography introduced in the 90s [55–57]. The algorithm for solving the nonlinear inverse problem is in most cases based on a Newton scheme, which is an iterative optimization process where the simulated scattered field from the current dielectric properties distribution is compared to the measured scattered field. The problem is solved to obtain quantitative images of an object. Several implementations of the Newton algorithm have been reported, one is the Newton-Kantorovich algorithm developed by Joachimowicz *et al.* [55], and has been used in the planar microwave camera (section 1.2.1), in an extended version [58, 59] for quantitative image reconstruction from experimental data. Other examples of the Newton based algorithm are the Gauss-Newton algorithm [60, 61] and the conjugate gradient algorithm [62]. All of these techniques mentioned above require a forward solver for calculating the scattered field, such as the methods of moments [55], the finite-element method [63] or the finite-difference time-domain method [62]. The heavy and large numerical calculation of the inverse formulation of the problem make this algorithm computationally expensive. Alternative algorithms utilize techniques to compensate for these problems, e.g. the multiplicative regularized contrast source inversion method, which have been successfully used for solving the nonlinear inverse problem by reducing the computational complexity. This algorithm has proven to be suitable for high contrast biological objects (tissues) and have been implemented in a number of different solutions [64–67].

The most frequently deployed algorithms for the radar approach is the confocal or delay-and-sum focusing algorithm [68–72]. The basic principles of this algorithm are a transmitted short pulse measured as a response in time at the receiver. The object of interest is divided into a number of pixels and the image is created by adding the time-delays for all received signals form the emitted pulse for each pixel. If a significant scatterer is present all scattered waveforms contain the scattered component signature. These waveforms are processed and summed from all antenna positions for a single pixel, which leads to a maximum of the signal (strong scatterer). The main advantages of this kind of algorithms is their simplicity, time efficiency and robustness.

1.3 Motivation

Breast cancer remains the most common cancer among women, with 30.4 percent of all female cancers according to recent Swedish statistic reports [73]. More than 90,000 women living in Sweden today have sometimes received a breast cancer diagnosis and 8490 diagnoses were made during 2012. The incidence has increased from about 80 to 180 cases per 100 000 over the period from 1970-2012. Globally the trends of incidences are similar [74].

Worth mentioning is that survival in cancer has been gradually improved, which has several explanations. New and improved methods of diagnosis, and prevention initiatives such as screening activity has led to more cases of cancer are detected early, which gives a greater chance for cure. The most successful tool used today for breast cancer screening is X-ray mammography, which in this case offers clear advantages [75, 76]. However, this technique also has some limitations and potential risks, where the breast is a subject to uncomfortable and painful compression and it uses ionizing radiation during the examination process. The breast compression also has the disadvantage that the tumors in the breast periphery near the chest wall may not be detected. Even though the ionizing radiation dose nowadays is low, the exposure poses a possible risk in an increased cancer risk.

Apart from those limitations, mammography also includes low sensitivity, the ability to identify a tumor presence, which is highly dependent on the radiologist experience, i.e. the human factor. The interpretations of Mammograms (X-ray images of the breast) are especially difficult for

dense breast (glandular/fibro-connective tissue), which is particularly common for younger women. The dense tissue impinging with the identification of abnormalities associated with tumors, complicating the radiologist's interpretation work and result in a higher rate of false-negative and false-positive test results in these cases. Another shortcoming is the specificity where the patients often needs additional examination techniques or a breast biopsy (invasive examination) to identify the findings from the mammogram as benign or malignant, and the specificity decrease with breast density. As a consequence of these shortcomings, mammography can have harmful impacts on the screened population.

These limitations of mammography have motivated research for complementary techniques for imaging breast cancer to secure minimal mortality in the future. Other available imaging techniques such as Ultrasound, positron emission tomography (PET) and Magnetic Resonance Imaging (MRI) are either less effective or are too costly for mass screening. For example, MRI offers higher sensitivity, but a trade-off with high cost and low specificity which may lead to over diagnosis.

There are many strong reasons that microwaves are assumed to be tractable in biomedical diagnostics: the contrast in constitutive parameters for different in-vivo tissues is higher for microwaves than the most successful tool used today X-ray computed tomography can produce. Furthermore, microwave frequencies are nonionizing and exhibit reasonable penetration depth in breast tissue. Microwave imaging might also be a mobile and cost-effective complement to current imaging techniques. This are the main reasons for microwave imaging being developed with potential as a complementary modality to mammography.

However, the current alternative imaging modalities to mammography suffer from their own challenges. In the case of microwaves for imaging purposes, the main disadvantage is microwaves itself due to their scattering nature. The problem is to extract information from the sensitive signals which certainly contains useful information. The research community faces many challenges, and in order to be competitive to other imaging modalities use the advantages of being cheaper and safer, the dynamic changes on the tissue properties is also an essential benefit to achieve this goal for microwave imaging. Hopefully in the near future the microwave community will overcome the challenges and provide complementary tools for the radiologist not only to diagnose but also treat cancer. This is a deserving cause and a noble task.

1.4 Outline of Thesis

The rest of this thesis is organized as follows. The problem formulation with the main defined research questions is presented in Chapter 2 together with the research method. Chapter 3 provides a brief overview of the algorithm deployed in our system. First, the direct problem is explained then following the image reconstruction algorithm based on the Newton-Kantorovich technique. In Chapter 4 parts of our research project and work is presented. The flexible robotic data acquisition system developed is described together with validation of the system and phantom development including permittivity measurements, moreover descriptions of the antenna and system calibration are provided. Finally, the quantitative image reconstructions from experimental data are given at the end of this chapter. In Chapter 5 a short description of the extended research project Mamacell is presented, following the focus on the antenna applicator design reasoning with the unveiled results in form of simulations. Chapter 6 summarizes the included papers and the contribution of the thesis. Conclusions and proposed ideas for future work are presented in Chapter 7.

Chapter 2

Problem formulation

The research of the group at Mälardalen University (MDH) is to investigate the usage of microwaves as a possible imaging method in biomedicine, which means to develop a measurement system for concept studies of microwave imaging modalities aimed towards a biomedical application. The aim is concentrated on using microwave imaging for breast tumour detection, but other potential applications within the area are planned for future works. The objective of this thesis can be formulated as follows:

"to develop a measurement platform system for microwave imaging and associated tool support towards biomedical applications"

Developing a microwave imaging system is a complex problem, which raises several questions needed to be examined. In order to refine this general research problem, we narrow our overall research goal into finer research questions. The following main research question (RQ) have been formulated as RQ 1-3.

RQ1 **How should a flexible system be designed for accurate measurements?**
One part of this thesis focuses on designing a flexible measurement platform able to scan an object of interest in different geometries. Hence, accurate measurements are required in order to conduct good quality data from the acquisition. The inverse scattering

problem will involve nonlinearity, causing ill-posed numerical computation. As a result, in particular applications, small perturbations in the measured data can cause large errors in the reconstruction process. Therefore the system also needs to be carefully calibrated.

RQ2 **How can the background medium and the material parameters for the phantom development be characterized with a reliable and repeatable method?**
To obtain precise control of the background medium, and a good estimation of the dielectric properties of materials mimicking human tissues there is a need to develop methods for permittivity measurement. In addition development of suitable reference phantoms is an important issue in order to evaluate and validate the systems performance in terms of quantitative image reconstructions.

RQ3 **Which antennas (sensors) should be used in the measurement systems?**
How to design antennas for other medium than air? This is the key question. The implementation of an efficient Microwave Imaging (MWI) system requires design and fabrication of suitable antennas, which is a significant challenge for this technique. Antennas are especially important as they are crucial for the efficiency of the imaging system. Typical design requirement from the literature studies involves small size, wide bandwidth, simple manufacturing as well as simple field equations, i.e. modeling. However, challenges for innovative, high performance antennas to be placed in contact or in close proximity with the imaged object, without the need of coupling liquids, demands the best possible narrowness of the antenna lobe, reduced influence by the surroundings, very small near-field effects, and small size.

These questions leave out the important areas of the reconstruction process and imaging algorithm, since the algorithm in this thesis is only used as a numerical tool without any contribution in this research domain. However a brief overview of the algorithm deployed in our system will be presented in Chapter 3.

2.1 Scientific Approach and Research Methods

In this thesis, the research is both within the area of technology and the area of science. Hence, the research can be seen as a bond between natural sciences, such as physics and mathematics, and the art of engineering.

Usually the research process begins with defining a problem and ends with proposing a solution to the problem. During the research process, the researcher may use one or several research methods in order to answer the established research questions. The process in this thesis begins with the identification and formulation of a general research problem by studying related work. A flow chart of the research process is shown in Figure 2.1, in which the main components are: defining the general research problem associated with related work, the formulated research questions, performing the research work and ending with validation. The main goal is to provide a solution to the practical problem, where the solution is obtained by narrowing down the general problem in form of refined research questions. A research work is an iterative process allowing feedback between stages. It starts with separation of the overall research idea into smaller research goals, which are formulated, studied and refined. In the research work stage, the tasks have been performed iteratively by collecting and analyzing data following up with analyzing and concluding the results. In some cases the research questions can be updated and extended by new research challenges. Once the research results are good enough, we carry on with the validation process as a final stage. The validation stage is the key part of this process, which assures the scientific value of the established research results. In case of failure in the validation stage, we have to go back and look over the research results, improve them if possible otherwise discard the results.

In order to understand the scientific problem, we have studied the state of the art gathering information from previous work done in the research area. During this stage, we have used the research method called *literature studies*. The purpose of literature research is to explain the problem and to see what other attempts have been like. The literature material relevant to our research that has been studied is journals, proceedings, books and the internet.

Other scientific methods used in our research project is the *induction*

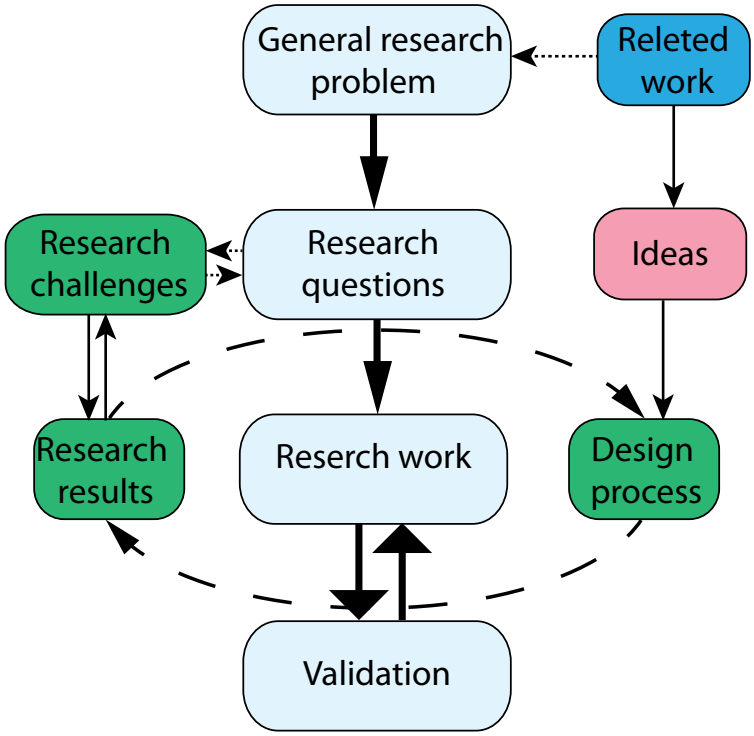

Figure 2.1: Flow chart of the research methodology process.

method which means that experimental results will be used to create theories. In addition, to be able to answer and validate the formulated RQ empirical measurements are needed, which is a *hypothetic deductive method*. Numerical modeling, as well as measurements, are the foundation from which theories will be built.

Chapter 3

Numerical Tool

The main objective of this chapter is to describe the imaging algorithm deployed for our system by introducing the direct, and inverse scattering problem as a model based illustration technique.

In microwave imaging, an inhomogeneity of the material will affect an incident field to scatter, due to the contrast in the constitutive electromagnetic parameters, i.e. the complex permittivity of the imaged material. Usually in a microwave imaging system the object of interest is embedded in a background medium with a cretin permittivity and conductivity representing the imaging domain. The object is illuminated by an incident field, E^i, emitted from a transmitting antenna, producing a scattered field E^s. The total field, E^t, measured by the receiving antenna is the sum of the incident field and the scattered field as following $E^t = E^i + E^s$. The total field will change by the scattered field introduced and thus the complex permittivity contrast distribution of the object can be obtained. The fundamental equations for describing electromagnetic phenomena in a physical environment is Maxwell's equations, which in this case will be converted to the wave equation.

The most common electromagnetic computational techniques used to implement the wave equation into the direct problem are Method of Moments (MoM), Finite Element Method (FEM) and Finite Difference method (FDM). These numerical techniques have had an important role during the last decades within computational modeling, where the availability of high performance computers made this possible. Depending on the electromagnetic problem to be solved numerical techniques

which have their foundation in mathematics, are chosen for the specific electromagnetic scenario. Typical scenarios in the area of electromagnetic modeling to mention a few are electromagnetic field distributions, scattering problems and antenna design. Further, the problem scenarios above may be characterized by the way they use frequency or time-domain. Another technique used in this thesis, as a tool for antenna design simulations and field pattern analysis, is based on a FDM in time domain, i.e. the Finite Difference Time Domain (FDTD). A commercially available software called QuickWave© for electromagnetic design and simulations based on the conformal FDTD, has been used extensively throughout paper E.

In the next section an imaging algorithm is presented for solving the direct, and inverse electromagnetic scattering problem due to a model based illustration method within the microwave range.

3.1 Direct Problem

Solving Maxwell's equations for a 3D version of the problem, field properties along all three dimensions, leads to heavy computational 3D vectorial problem. For the direct electromagnetic formulation, we have used a classical approach considering a 2D scenario of the problem. In the 2D formulation, the object of interest is considered to be nonmagnetic with constant dielectric properties along its vertical axis. In this method the electromagnetic scattering problem is converted into a radiating problem in free space, and a 2D scalar Electrical Field Integral Equation (EFIE). The implicit time dependence is introduced as $e^{-j\omega t}$, with ω as the radial frequency. The homogeneous,- and inhomogeneous wave equation in this context are described, by the scalar Helmholtz equation [59], respectively as

$$(\nabla^2 + k_1^2)e^i(\vec{r}) = 0 \tag{3.1}$$

and

$$(\nabla^2 + k^2)e(\vec{r}) = 0 \tag{3.2}$$

where, $e^i(\vec{r})$, incident field is the propagation of a TM-polarized, single-frequency, time-harmonic electromagnetic wave and $e(\vec{r})$ is the total electrical field. The constant wavenumber k_1 inside the homogeneous media, and the wavenumber k, which depends on the dielectric properties of the

medium of propagation, are

$$k_1 = \omega\sqrt{\mu_0\epsilon_1^*} \tag{3.3}$$

and

$$k^2 = \omega^2\mu_0\epsilon^*(r) \tag{3.4}$$

where ϵ_1^* is the complex permittivity inside the homogeneous media, and $\epsilon^*(r)$ being the complex permittivity of the inhomogeneous region. The total field $e(\vec{r})$ in equation (3.2) can be seen as a superposition of the incident field, $e^i(\vec{r})$ (without the object), and the scattered field $e^s(\vec{r})$ (caused by the object), written as

$$e(\vec{r}) = e^i(\vec{r}) + e^s(\vec{r}) \tag{3.5}$$

Defining the contrast $C(\vec{r})$ as

$$C(\vec{r}) = k^2(\vec{r}) - k_1^2 \tag{3.6}$$

and introducing equation (3.5) together with equation (3.6) above into equation (3.2) will result in the following wave equation

$$(\nabla^2 + k_1^2)e^s(\vec{r}) = -C(\vec{r})e(\vec{r}) \tag{3.7}$$

The scattered field in equation (3.7) is related to an equivalent current $J(\vec{r})$ as

$$J(\vec{r}) = C(\vec{r})e(\vec{r}) \tag{3.8}$$

In order to solve $e^s(\vec{r})$, a Green's function formulation for the inhomogeneous scalar Helmholtz equation in (3.7) is introduced.

$$(\nabla^2 + k_1^2)G(\vec{r}, \vec{r\prime}) = -\delta(\vec{r} - \vec{r\prime}) \tag{3.9}$$

The Green's function represents the scattered field radiated by a line source, and is defined as $j/H_0^{(1)}(k_1|\vec{r} - \vec{r\prime})|)$ where $H_0^{(1)}$ is the zero-order Hankel function of first kind. The index r and $r\prime$ represent the observation and source points, respectively. By using Green's function formulation above and the principle of superposition, the scattered field can be deducted by

$$e^s(\vec{r}) = \iint_S G(\vec{r}, \vec{r\prime})C(\vec{r\prime})e(\vec{r\prime}) \tag{3.10}$$

The total field, considering equations (3.5) and (3.10), is expressed as the following integral formulation

$$e(\vec{r}) = e^i(\vec{r}) + \iint_S G(\vec{r}, \vec{r\prime}) C(\vec{r\prime}) e(\vec{r\prime}) \tag{3.11}$$

The incident field $e^i(\vec{r})$ is given and the complex permittivity is known, the scattered field $e^s(\vec{r})$ will be computed as the direct formulation of the electromagnetic scattering problem. In such context, equations (3.10) and (3.11) are numerically implemented and solved by MoM [55, 56, 77, 78]. By this numerical method, a two-dimensional configuration, by cylindrical situated monopoles, is solved in this thesis. By assuming constant fields and dielectric properties in a rectangular cell as the imaged object, the incident,- and the scattered field will be discretized as

$$e^i(\vec{r_n}) = \sum_{j=1}^{N} [\delta_n j - G(\vec{r_n}, \vec{r_j}) C(\vec{r_j})] e(\vec{r_j}), \quad n = 1, 2, ..., N \tag{3.12}$$

and

$$e^s(\vec{r_m}) = \sum_{j=1}^{M} [\delta_n j - G(\vec{r_m}, \vec{r_j}) C(\vec{r_j})] e(\vec{r_j}), \quad m = 1, 2, ..., M \tag{3.13}$$

where the object region is discretized into N cells and also M receiving points for the observed scattered field. Numerical solution of this direct scattering problem will be used for creating image reconstruction algorithms for the inverse problem from which the unknown permittivity contrast distribution of the object will be found.

3.2 Image Reconstruction Algorithm

In order to produce a tomographic image of large high contrast objects the inverse electromagnetic scattering problem should be solved. In this process, the unknown complex permittivity distribution of the object is deduced from the measured scattered field due to the object and a known incident electric field. A number of imaging modalities have been used for solving the nonlinear inverse scattering problem and in most cases using an algorithm based on the iterative optimization process. In each iteration, the scattered field from the current parameter distribution is

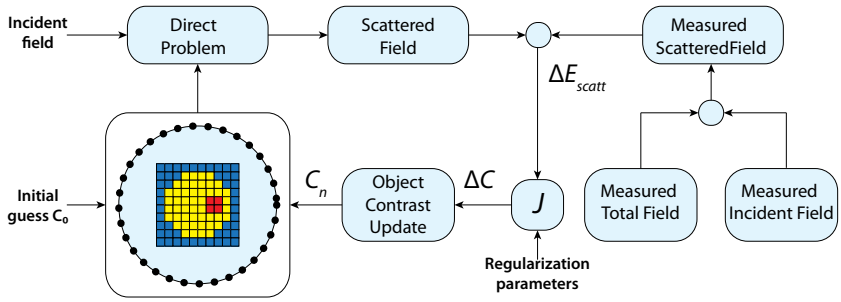

Figure 3.1: Flow-chart of the NK algorithm

computed from the direct problem and compared to the measured field. The difference between the measured and computed scattered field is minimized until the error is sufficiently small and a stability criterion is reached. This optimization process can be implemented in a Least Square formulation called Newton-Kantorovich (NK) [55].

The 2D scalar NK code, has been used (in an extended version), as a numerical tool for solving the 2D scalar nonlinear inverse scattering problem [59]. Before computing the scattered field the total field inside the N cells of the object must be calculated by solving Equation 3.12 in previous section (3.1). The relation between the scattered field and the contrast permittivity of the object is nonlinear. The Equations 3.12 and 3.13 can be written in matrix form and the scattered field can be expressed as:

$$E_{scatt} = K_{R,O}[C][I - CK_{O,O}]^{-1}E_{inc} \tag{3.14}$$

The residue is defined as a difference between the calculated scattered field E_{scatt}, and the measured scattered field E^{meas}_{scatt} as:

$$\Delta E_{scatt} = \mathbf{E}_{scatt}(C_n, r) - \mathbf{E}^{meas}_{scatt}(r) \tag{3.15}$$

Solving the nonlinear inverse scattering problem, the solution is obtained iteratively by minimizing the square norm of the error between the computed scattered field and the measured field:

$$min\|\mathbf{E}_{scatt}(C_n, r) - \mathbf{E}^{meas}_{scatt}(r)\|^2 \tag{3.16}$$

where C_n contains the estimate of the object's dielectric property distribution at iteration n. Applying regularized Gauss-Newton, gives a linear relation between the dielectric contrast update step ΔC and the residue ΔE^{scatt} at iteration n as:

$$\big(J^* J + \mu I\big)\Delta C = J^* \Delta E^{scatt} \tag{3.17}$$

In Equation 3.17, J is the Jacobian matrix of $\mathbf{E}^{scatt}(C_n, r)$, also called the sensitivity matrix, and J^* its conjugate transpose matrix. The regularization-term, μ, is introduced to decrease the condition number of the J^*J matrix, which is essential to avoid false solutions and obtain convergence of the iterative process [79]. As can be seen in Figure 3.1, the iterative process starting with an initial contrast distribution C_0, the difference between the computed and measured scattered field gives the residue ΔE_{scatt}. The estimation of the contrast function step ΔC, is done using the Equation 3.17.

Chapter 4

Resarch Project Description

In this chapter, our research project and work at MDH is presented. The experimental robot controlled acquisition system developed is described together with validation of the system and preliminary simulations. Following the phantom development, antenna design and performance, system calibration and finally image reconstructions from experimental data. This chapter of the thesis is tied to and deals with issues related to all three RQ.

4.1 System Overview of Robot Controlled Microwave Imaging System

Development of experimental systems able to generate data for providing the algorithms has encountered a growing attention, especially in the last decade. The design of the MWI system at MDH is based on the literature study from the previous works, mentioned in Chapter 1 and section 1.2, in particular the circular systems developed by Meaney *et al.* and Semenov *et al.*. Also, the experiences gained from the planar microwave camera, section 1.2, have been taken into consideration during the design process.

The challenge to design and develop a new feasible system, relating to the previous MWI systems and research works, a flexible multi-frequency

Figure 4.1: The MDH experimental setup for the robot controlled MWI system. The receiving antenna is mounted on the robot's sixth axis with the tool extension (in right photo I), and the transmitting antenna (in right photo II) is on a fixture in the water-filled tank. The object is placed on rotational board controlled by a stepper motor, the computer with the controlling interface and VNA glimpsed outside the water tank in the left photo. A close-up of the breast phantom surrounded by receiving antenna (I), transmitting antenna (II) and the ultrasonic sensor (III) is shown in the right photo.

MWI system was realized. Intended as a measuring platform system able to be used in both hardware (antennas and system geometry) and algorithmic investigations for future MWI systems.

The measurement system utilized for microwave imaging at MDH consist of an ABB® robot with the model number IRB140, capable of moving in six degrees of freedom (six independent rotational axis). Two photos of the system arrangement during the measurement of the breast phantom is shown in Figure 4.1. The system also includes: two identical monopole antennas where the receiving antenna is mounted on the tip of the robot arm and the transmitting is attached to the main fixture as shown in Figure 4.1 right. Both antennas are immersed in a water-tank (filled with tap water) with a diameter of 2 m and in which an object-fixture has been placed in the center. In addition it is comprised of an ultrasonic sensor, a stepper motor, a Rohde & Schwarz ZVB 8® Vector Network Analyzer (VNA) connecting directly the transmitting and receiving antennas to port 1 and 2, respectively and a developed Matlab® interface controlling the entire system.

The object of interest is mounted on a fixture with a rotational axis controlled by a stepper motor to simulate multi-view imaging at dif-

ferent angular positions of the transmitter and the synthetic receiving antenna array. The receiving antenna is attached to the sixth robot axis with a tool extension able to move along planar, cylindrical or half-spherical surfaces around the object of interest. In Paper D section II-B, is the details regarding the receiving antenna geometry explained. Several parameters are adjustable for the different geometries, as the radius, angular steps and the number of frequency measurement points. A multi-view examination is possible using the stepper motor, taking angular steps as small as 1.8°. This is equivalent of having a rotation of the antenna; thus a synthetic receiving antenna array rotated with the transmitting antenna is obtained. In addition, an ultrasonic sensor is attached to the tool extension for calibration of the system's center-point in relation to the rotational axis. The ultrasonic sensor could also be used to get a priori information from the object's surface to be used in the inverse algorithm. The transmitting antenna is arranged in a way that it can be moved manually in different directions along the fixture and, in the normal setup, it can be fixed at one position throughout the examination.

A data acquisition program controls the instruments and the robot. During a measurement, the control interface will receive wide-band measurements from the GPIB connected VNA at each measurement position. First, the incident field (without the object) is measured before the total field (with the object present) is measured; this is obtained in form of complex S_{21}-parameters from which the amplitude and phase are calculated. The control interface stores data from both fields, and the scattered field can be computed by subtracting the incident field from the total field.

There are several advantages of the proposed robot controlled measurement system, where the most important one is fulfilling the accuracy and flexibility according to the formulated RQ 1. Using a robot system, the receive antenna can be positioned with very high precision, with an absolute error less than 0.1 mm and even better repeatability. Also, the possibility to utilize the robot's degrees of freedom forming synthetic arrays of different geometries making the system flexible. Having flexible receiving antenna positions enables investigations to be made of different antenna array geometries without introducing coupling effects between multiple antenna elements in the system design stage [80]. Furthermore, examination of the most suitable frequency for the imaging application by obtaining rapid wide-band measurements is an advantage with such

a system.

This flexibility enables investigations on different synthetic antenna array geometries and frequency usage for different imaging applications, without introducing coupling effects between multiple antenna elements in the system design stage

The large water-tank will attenuate the reflected signals from the surroundings in the tank which can be neglected and the disturbances by scattering objects outside the tank do not influence the system. However, there are no opportunities for changing the matching liquid (background medium) adjusting it to investigations of different imaging scenarios. This is a negative factor to consider. Another disadvantage of the system is the inability to adjust the complex permittivity and temperature of the background medium, since the volume is large.

4.2 Preliminary Experimental Validation

This section is a part of the work presented in Paper A, and our preliminary validation of the MWI system intended as a meaningful experimental platform for microwave imaging scenarios. The first experimental validation is performed by using a sunflower oil ($\varepsilon^* = 2.5 + j0.1$) polycarbonate (PC) cylinder with a diameter of 110 mm (3 mm thick), placed on the object fixture in the tank filled with 10°C water ($\varepsilon^* = 83.2 + j7.3$). The measurement configurations of the MWI system are set to cylindrical with a radius of 225 mm, and the receiving antenna is sweeping a circular arc of 270° with the step size of 5° between each measurement point giving 55 receiving points. The transmitting antenna is located 114 mm from the center at 0° in angular position. For the sake of validation of the experimental MWI system the direct solver described in section 3.1 is used and configured for a cylindrical incident field. In Figure 4.2, the comparison between the simulated and measured scattered field at 1 GHz is pointed out. As one can see the phase, right Figure 4.2, has almost a perfect fit with a root mean square (RMS) error less than 14°, while the amplitude have small differences on the left of Figure 4.2, and a RMS error between the simulated and measured data less than 1.6 dB.

In order to see the MWI systems capability in the framework of breast tumour detection, a preliminary simulation is performed for the cylindrical geometry described above. The complex permittivity values

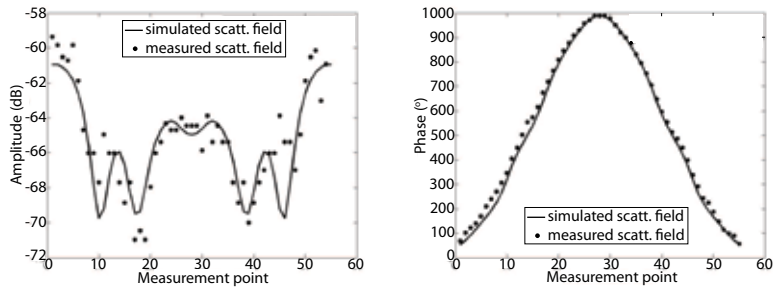

Figure 4.2: Comparison between the measured and computed scattered field from a sunflower oil filled 110 mm diameter polycarbonate cylinder at 1 GHz, amplitude(left), unwrapped phase (left).

for the simulated breast phantom (110 mm diameter PC cylinder) corresponds to an average of three different adipose tissues [81, 82] with $\varepsilon^* = 34 + j11.5$. For the simulated tumor phantom (16 mm diameter), the complex permittivity is set to $\varepsilon^* = 57.4 + j17.4$. The frequency is chosen to be 1 GHz and the background medium is considered as tap water (10°C) with a complex permittivity of $\varepsilon^* = 83.2 + j7.3$. The phantom is discretized into 27×27 cells with a wavelength of $\lambda/7$ for a single cell size. The NK code, presented in section 3.2, has been used for the image reconstruction process with an applied Gaussian distributed noise. The reconstructed image can be seen in Figure 4.3 during the iterative process starting with the initial guess of a breast without a tumor, going through four iterations and ending with the expected value. As can be seen both the real and imaginary profiles are well reconstructed for the given settings, and the best results are obtained after three iterations.

Following steps in the research work are related to phantom development with permittivity measurements and the characterization of the image reconstruction capabilities of the system from experimental data.

4.3 Phantom Development

Phantoms that mimic human tissues have been of great importance for the development and testing of different medical imaging modalities. Extension of the work done in Paper A is concerning the reconstruction of

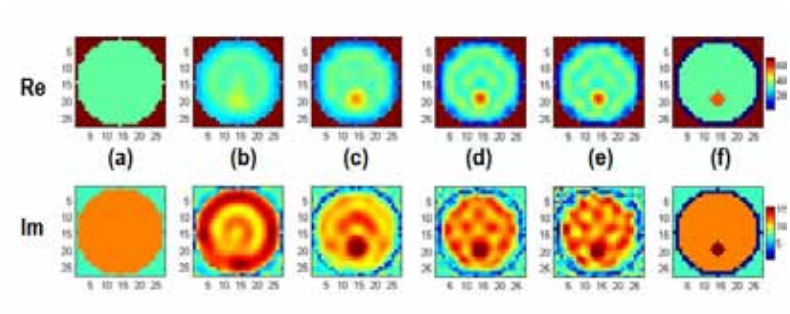

Figure 4.3: Reconstructed real- and imaginary permittivity profile of the numerical breast phantom with a SNR of 40 dB, starting with (a) the initial guess, (b), (c), (d) and (e) iteration 1, 2, 3, 4 respectively, and (e) expected profile.

multi-view data from an inhomogeneous object to test the MWI system's ability in terms of quantitative imaging. In order to perform this challenge, a realistic breast phantom is developed, which needs a reliable and repeatable method for characterization of materials dielectric properties. This is a part associated with RQ 2.

Our motivation with this work is realization of a simple breast phantom for our designed and validated robot controlled MWI system. The goal is to find suitable materials able to mimicking normal breast and tumor tissue.

Previously reported studies [83–86] of the contrast in dielectric properties of ex vivo measurement between normal and malignant human breast tissues at microwave frequencies has gained a base for researchers on using microwaves for breast tumor detection. The result from these measurements showed a contrast of approximately 4:1 between normal and malignant breast tissues and in some cases as large as 10:1. In the most recent studies, the reported contrast in dielectric properties between normal and malignant breast tissues was presented in details by Lazebnik and her colleagues (joint study at the University of Wisconsin and the University of Calgary) [81, 82]. They conducted a large-scale study measurement characterizing the dielectric properties, at a frequency range from 0.5 to 20 GHz, of excised normal, benign, and malignant breast tissues obtained from breast reduction and cancer surg-

eries. From these measurements, it has been concluded that there is a large variation in dielectric properties of normal breast tissue due to the considered tissue heterogeneity [81], and a ratio as large as 10:1 between malignant and normal adipose tissues [82]. However, the same studies show that the contrast is reduced to approximately 10 percent between malignant and normal glandular breast tissues. This imposes a greater challenge on the design of MWI system that will be able to detect the small contrast of 10 percent differences in breast tissue dielectric properties.

Breast phantom development involves measurements of dielectric properties of different materials (fluids) and mixtures. The dielectric properties of materials can be measured with several cavity resonance methods [87]. Methods for measuring the complex permittivity of lossy liquids at microwave frequencies are especially interesting because lossy dielectric liquids can match the permittivity of biological tissues very well. The resonant cavity perturbation method is a commonly used technique for the complex permittivity measurements, i.e. the relative permittivity and loss factor (conductivity). The sample to be studied is introduced into a cylindrical resonant cavity, and its complex permittivity is determined from the shift of the resonant frequency and the change of the cavity quality factor (Q-factor). The advantage with the cylindrical cavity in comparison to other rectangular cavities is that it offers higher Q-factor and, therefore, higher accuracy. For our measurements, a so called reentrant cavity have been used and is presented with a feasibility study in detail in Paper B. The cavity method in this study proved to have a repeatability of the measurement system limited to approximately a permittivity difference of 2 units, which is slightly better than the commercially available coaxial probe. Nevertheless, in the case at hand the decision taken later on was to use the open-ended coaxial probe for the possibility of rapid measurements and convenience simplifying the work.

The first breast phantom was created by using a Plexiglas cylindrical structure filled with 50 percent 1.2-propylene glycol, and 50 percent distilled water mixtures (simulating breast tissue), agar was added for obtaining a jelly like materials. A smaller Plexiglas tube, filled with the same mixtures but different proportions and added salt, was placed inside the bigger cylinder in order to simulate tumor tissue. Image reconstructions were performed with the phantom, in the planar microwave imaging system, described in section 1.2.1, by researchers at Suplec in Paris. These experiments showed an incorrect value of the imaginary

Figure 4.4: The breast phantom mounted on the object fixture's rotational axis with one smaller cylinder mimicking tumor tissue (left), and phantom with two smaller cylinders mimicking tumor tissue and an anomaly in the breast(right).

part of the phantom's complex permittivity. The jelly based phantom proved to create a material with high losses, which is a consequence of a chemical reaction when mixing 1.2-propylene glycol with water. The conclusion is that the 1.2-propylene glycol is inappropriate to use as a breast phantom material for the purpose of image reconstruction.

The second breast phantom is materialized as simplified cylindrical structure using homogeneous materials, mixture of the surfactant Triton X-100 and deionized water [59], mimicking the breast tissue and tumor. The breast phantom consists of two polycarbonate (PC) cylinders shown on the left of Figure 4.4, filled with a mixture of deionized water and surfactant Triton X-100 for the breast tissue, same for the smaller cylinder representing the tumor tissue with added salt. As a starting point the work by Lazebnik *et al.* [81] was used to set values for the breast phantom, and these values represent an average of three different breast tissues resulting in a complex permittivity $\varepsilon^* = 35.6 + j7.3$ (50% of Triton X-100). The cylinder holding the normal breast tissue is 110 mm in diameter with a 2 mm thick PC material. And the tumor fluid (20% Triton X-100 with 0.5% added salt adjusting the imaginary part, $\varepsilon^* = 58.6 + j15$), is poured in a smaller PC structure with a 20 mm diameter and 2 m thick material placed inside the breast tissue mimicking material. This phantom is used in Paper C as a realistic breast

phantom to compare two antenna design and examine the MWI system's ability in term of quantitative imaging.

Later on another similar phantom was created with an additional small PC cylinder (20 mm diameter and 2 mm thick) positioned inside the breast material and filled with deionized water shown on the right of Figure 4.4. The material characteristics and dimensions of this phantom is exactly the same as the one described above except the new small PC structure simulating one more anomaly in the breast. In Paper D this phantom is used for the experiments and image reconstructions.

4.4 Antenna Choice, Design and Performance

The antennas are obviously one of the most important part of the imaging system, and their design is essential for the system's sensitivity. Using model based optimization in microwave tomography algorithms, such as NK, it is crucial that the antenna can be modelled accurately with a quite simple antenna model, to lower the computational burden without increasing the model errors. Model errors will drive the image reconstruction into false solutions. With this objective in mind, we have started with a simple monopole antenna with a ground plane as the initial antenna design. Using a monopole antenna in the system has the advantage of being easily modeled as a line source in a 2D imaging problem [31, 88]. In addition, the antenna is compact and can be placed around the breast model in a number of different and tight geometries. The linearly polarized monopole antenna design is used as both the transmitter and receiver antennas. Two identical monopole antennas were fabricated using a semi-rigid coaxial cable with a physical length (L) of the exposed part (center conductor) of 11 mm, $\lambda/4<L<\lambda/2$. The first antenna design was with a ground plane where four wires formed a cross, and the length of one wire was 25 mm as shown in Figure 4.5 left.

The problem with this design, however, is that the orientation of the receiver must be maintained at a certain angle to the transmitter to obtain an incident field as close as possible to the model. That was done by fine-tuning the antennas by hand, rotating them around their own axis and fitting the amplitude of the measured incident field to the amplitude of the simulated incident field model.

The second design was a monopole antenna with a circular ground

Figure 4.5: Antennas mounted on the robot arm: antenna with the cross ground plane (left), and antenna with a circular ground plane (right).

plane with a radius of 9.5 mm shown on the right of Figure 4.5, and a rotationally symmetric radiation pattern in the horizontal plane, eliminating the need to tune the antenna manually. The antenna is fed through an N-type to SMA connector with a power of 13 dBm from the network analyzer. The return loss in water at a temperature of 20°C and a permittivity of approximately $\varepsilon^* = 77 + j7$, is shown in Figure 4.6. Both the measured and simulated S_{11} results are shown, and it can be seen a good level of agreement between the two arrangements of data. The return loss is below -14 dB at around 1 GHz with a bandwidth of approximately 200 MHz. In a later experiment, the frequency bandwidth was improved by putting a sleeve on the tip of the antenna.

A small antenna, like in our case the small monopole antenna, has a capacitive overflow. When the antenna is surrounded by a high permittivity material, the result is even a higher capacitance, which is not desirable, because there is no magnetic material present that could match this. If, instead, a small dielectric sleeve is used as a cover over the protruding tip of the antenna, then the capacitance will decrease because the antenna is "further away" from the surrounding medium and the matching will be better. Another thing is if the antenna is 11 mm (physical length) and it is surrounded by water with a permittivity value of near 81, which will give a wavelength that is 9 times smaller so around 30 mm at 1 GHz. The physical length of the antenna is between $\lambda/4 < L < \lambda/2$, which will make the wave propagate more upwards.

With the sleeve on the antenna, the radiation pattern is more focused in the imaging plane. The reason for this is that the antenna, electrically seen, is longer because there is less capacitance when using the sleeve, which represents more inductance improving the overall function. The

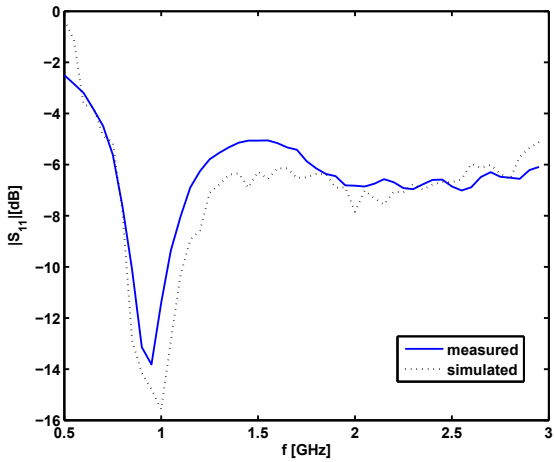

Figure 4.6: Measured and simulated S_{11} characteristics of the monopole antenna with the circular ground plane.

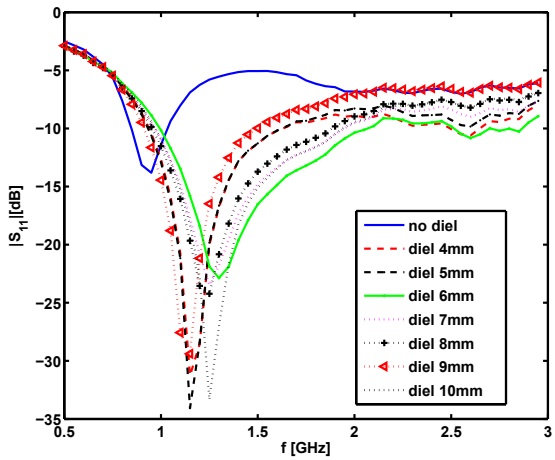

Figure 4.7: The measured S_{11} for the antenna both the return loss without the dielectric material on the tip and several scenarios with dielectric material.

facts mentioned above will affect the return loss of the antenna and improve the frequency bandwidth. In some cases, the antenna could be used for measurements up to 3 GHz with the return loss around -10 dB, see Figure 4.7. Measurements have been conducted with this new antenna using the case with a dielectric sleeve length of 6 mm (best frequency bandwidth for the antenna), and image reconstructions are compared to the other antenna design and presented in section 4.7.

4.5 Data Acquisition

A Matlab® program is used to control the data acquisition, coordinate the robot and communicate with the VNA. The object under examination positioned in the water-tank was illuminated by the electromagnetic wave from the transmitting antenna and the receiving antenna collected the scattered field at different locations controlled by the robotic system.

The fields were measured with the VNA in terms of the complex scattering parameters (S-parameters) between the transmitter and the receiver. The particular scattering parameter used is S_{21}, where the indices 1 and 2 refer to the transmitter and receiver, respectively. This is repeated for each receiver position and stored in the Matlab® interface as equations (4.1) and (4.2).

$$\mathbf{E}^{inc}_{meas}(r) = \Phi(r) \cdot S^{inc}_{21} \tag{4.1}$$

$$\mathbf{E}^{tot}_{meas}(r) = \Phi(r) \cdot S^{tot}_{21} \tag{4.2}$$

Equation (4.1) is related to the incident field $\mathbf{E}^{inc}_{meas}(r)$ without an object in the imaging domain. The total field when the object is present in the imaging domain is stored as equation (4.2). The index r represents the receiving points. $\Phi(r)$ is a complex calibration vector representing the unknown amplitude and phase difference between the experimental system and the numerical model, described in subsection 4.6.2. The measured scattered field $\mathbf{E}^{scatt}_{meas}$ attributable to the object can be derived from the incident and total field according to equation (4.3).

$$\mathbf{E}^{scatt}_{meas}(r) = \mathbf{E}^{tot}_{meas}(r) - \mathbf{E}^{inc}_{meas}(r) \tag{4.3}$$

4.6 System Calibration

In order to fulfil the requirements of RQ 1 and work towards the overall research goal, the system needs to be properly calibrated, as well as validating the accuracy of the MWI system.

The NK algorithm minimizes the error in an iterative manner between the measured and the computed scattered field from a numerical model in the direct problem. As a result, the solution is highly sensitive to errors in the incident field model inside the object region and to antenna positioning errors. The numerical incident field must agree with the measured field from the experimental setup. Moreover, since the measurements must be done with the coordinate system of the object's rotational axis in the centre and the robot has its own coordinate system, calibration is needed to make sure no position errors are introduced in the synthetic antenna array.

An accurate value for the complex permittivity of the background medium is one crucial parameter together with the incident field distribution for reduction of the model errors. With this in mind the antennas in the system are also used for estimating the permittivity of tap water, as well as, to determine an accurate incident field.

The model errors mentioned are minimized through a calibration process, presented in Paper D and parts of Paper C, described in following sections.

4.6.1 Background Permittivity Estimation

Tap water with different temperature was used as a background medium, and the theoretical model developed by Stogryn could be used to estimate the complex permittivity knowing the temperature and the salinity [89]. However, to have a more accurate estimation of the complex permittivity, a measurement based method is preferable as this eliminates errors in the reconstruction process. Method proposed uses the electric field from N number of measurement points from the monopole antenna moved along a line of propagation from the transmitter, to estimate the dielectric properties of any background medium. The measured transmission data is represented as a logarithmic amplitude and unwrapped phase distribution along a line, as depicted in Fig. 4.8, and, using a least squares (LS) model a straight line is found to fit the measured data with very good accuracy.

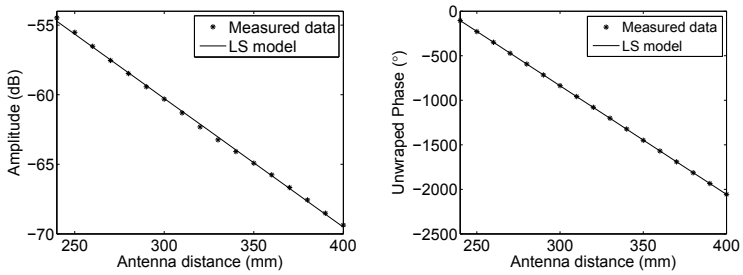

Figure 4.8: The measured complex transmission data between the antennas (from 240 mm to 400 mm sampling every 10 mm) fitted with the LS first-order polynomial, representing the logarithmic amplitude $\hat{A}$ (left) and unwrapped phase $\hat{\theta}_{deg}$ (right).

The radiated field from the antenna is a cylindrical wave, but looking in one point in the far field, we can consider plane wave propagation as:

$$\mathbf{E}(x) = Ae^{-jk_1 x} = Ae^{-j(k_1' + jk_1'')x} \tag{4.4}$$

From Fig. 4.8, the complex wave number k_1 is obtained from the slope of the amplitude and phase curves. The coefficient k_1' is calculated from the slope of the unwrapped phase curve, Fig. 4.8 using:

$$k_1' = \frac{\pi}{180}\frac{\partial \hat{\theta}_{deg}}{\partial x} \tag{4.5}$$

The imaginary wave number, k_1'' is found by differentiating the logarithmic amplitude:

$$\frac{\partial A_{dB}}{\partial x} = 20k_1'' \log_{10}(e) \tag{4.6}$$

Using the equation for the wavenumber in combination with equations (4.5) and (4.6) the complex permittivity $\varepsilon^* = \varepsilon' + j\varepsilon''$ is obtained:

$$\varepsilon' = \frac{(k_1')^2 - \left(\frac{\frac{\partial A_{dB}}{\partial x}}{20\log_{10}(e)}\right)^2}{(2\pi f)^2 \mu_0 \varepsilon_0} \tag{4.7}$$

Frequency (MHz)	Measurement	Stogryn's model
Temperature 12.1°C		
950	$\varepsilon' = 81.93; \varepsilon'' = 6.25$	$\varepsilon' = 82.53; \varepsilon'' = 6.25$
1140	$\varepsilon' = 81.49; \varepsilon'' = 7.09$	$\varepsilon' = 82.36; \varepsilon'' = 7.19$
1500	$\varepsilon' = 80.22; \varepsilon'' = 8.65$	$\varepsilon' = 81.96; \varepsilon'' = 9.06$
Temperature 20.6°C		
950	$\varepsilon' = 79.73; \varepsilon'' = 5.88$	$\varepsilon' = 79.64; \varepsilon'' = 5.98$
1140	$\varepsilon' = 79.03; \varepsilon'' = 6.50$	$\varepsilon' = 79.54; \varepsilon'' = 6.50$
1500	$\varepsilon' = 78.97; \varepsilon'' = 7.60$	$\varepsilon' = 79.30; \varepsilon'' = 7.67$

Table 4.1: Permittivity measurements compared to Stogryn's model

$$\varepsilon'' = \frac{2k_1' \frac{\frac{\partial A_{dB}}{\partial x}}{20\log_{10}(e)}}{(2\pi f)^2 \mu_0 \varepsilon_0} \tag{4.8}$$

Inserting the experimental values into equations (4.7) and (4.8), gives a complex permittivity for the background medium and compared to the estimated theoretical complex permittivity value from Stogryn's model [89] are presented in Table 4.1. The results prove the experimental method to be good for estimating the background medium for the MWI system.

4.6.2 Incident Field Calibration

The validation of the incident field model has to be performed in order to match the measurements to the model. The measured incident field must agree with the numerical incident field model, where the transmitted field signals have to be validated in both amplitude and phase. A reference measurement is needed for the incident field, without the breast phantom in the imaging domain. This is compared to the computed incident field. In the numerical incident field model of the algorithm, the radiated field from the antenna is modeled as a vertical polarized cylindrical wave emitted by a line source according to equation (4.9).

$$E_{inc}(r) = -\frac{\pi}{2} f \mu_0 H_0^{(1)}(k_1 |r - r'|) \tag{4.9}$$

The expression $H_0^{(1)}(k_1|r - r'|)$ is the zero-order Hankel function of the first kind, k_1 is the wave number of the background medium calculated

in the previous section, r and r' represent the observation and source point, respectively, and f is the frequency.

A validation of the incident field model in one view is shown in Figure 4.9, where the simulated incident field is compared to the measured incident field at the receiving points and, as can be seen, the measured incident field is well matched in both amplitude and unwrapped phase. It is concluded that the antenna with the circular ground plane has a better match for the measured incident field in both amplitude and phase. Figures for the other monopole antenna design is not shown here, but can be found in Paper C section 4.

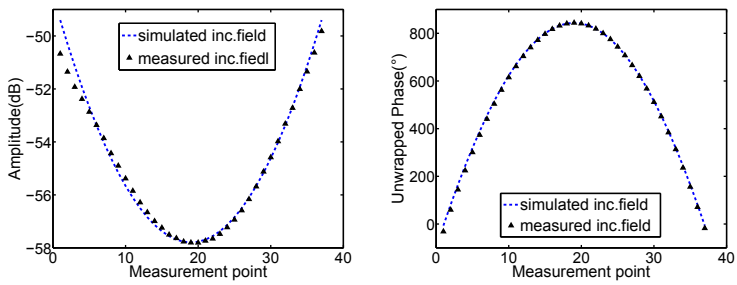

Figure 4.9: Comparison between the incident field model and the measured incident field, amplitude (left), and unwrapped phase (right) for antenna with circular ground plane.

The complex calibration vector $\Phi(r)$, used for all measurements as in section 4.5, is then estimated as the fraction of the reference data sets as [88]:

$$\Phi(r) == \frac{\mathbf{E}_{ref}^{sim}(r)}{\mathbf{E}_{ref}^{meas}(r)} \tag{4.10}$$

Before and after each series of measurement of the total field, a few samples of the incident field data are conducted. A comparison is carried out between these two incident fields in order to get an insight of the idea concerning the repeatability of the system performance during an examination process collecting total field multiview data. The calculated RMS error, before and after the data acquisition, at 1140 MHz is 0.15 dB in amplitude and 1.33° in phase, while for the lower frequency 950 MHz the RMS value is 0.12 dB in amplitude and 1.21° in pahse. Going up in

frequency will increase the RMS error between the incident fields before and after, and at 2 GHz, which is close to the noise floor the error is 0.6 dB in amplitude and 6.6° in phase.

4.6.3 Robot Coordinate System Calibration

The robot's coordinate system has to be calibrated to the origin of the object's rotational axis in order to minimize the position errors of the synthetic antenna array. To define the center point of the actual geometry to obtain the appropriate distance from the tip of the robot tool where the receiving antenna is positioned an ultrasonic sensor has been used highlighted in Figure 4.1 right (section 4.1). To calculate the center point of the rotational axis, the robot scans the cylinder and a number of distance measurements are stored. Then a mathematical model for calculating the center of a known cylinder from the distance measurements is implemented together with the Matalb® interface. The absolute error for the positioning system is calculated to be 0.46 mm. Details concerning this calibration process can be found in Paper D section IV-B.

4.7 Image Reconstruction using the MWI System

Here we present the quantitative 2D reconstructed images from experimental data measured with the robot controlled MWI system, described earlier in this chapter, using the numerical tool, i.e., the NK algorithm (chapter 3).

The first results represents comparison between the performances of the two monopole antennas with different ground planes using the incident field validation technique described in section 4.6.2. The phantom (left Figure 4.4) is based on the mixture of the Triton X-100 material (section 4.3) with the permittivity values of $\varepsilon' = 35.6$ and $\varepsilon'' = 7.3$ (50% of Triton X-100). This material simulating normal breast tissue is filled into the 110 mm PC cylinder and the tumor fluid (20% Triton X-100 with 0.5% salt $\epsilon' = 58.6, \varepsilon'' = 15$), is poured in the smaller PC structure placed inside the breast tissue mimicking material. The object region is discretized into 27×27 cells with a wavelength of $\lambda/7$ for a singel cell size. The cylindrical scanning pattern is utilized, and the scattered field is measured in the horizontal plane along a circular arc with a radius of

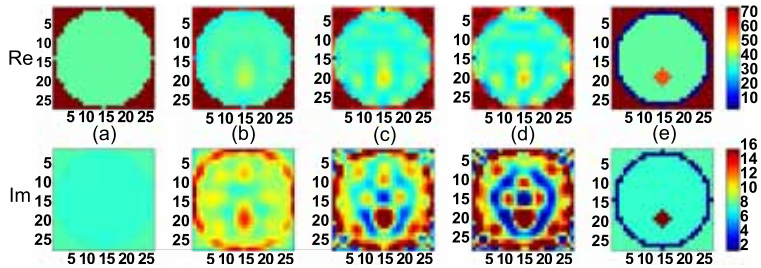

Figure 4.10: Reconstructed real and imaginary permittivity profile of the phantom in Figure 4.4 left using the antenna with the cross ground plane as in Figure 4.5 left. Starting with (a) the initial guess, (b), (c) and (d) iteration 1, 2, 3 respectively, and (e) expected profile. Frequency: 1140 MHz.

120 mm around the phantom. The receiving antenna attached via the tool extension to the sixth robot axis is moved in 37 points (on one half of the circular arc from 90° to 270° using 5° between each points), while the transmitting antenna is positioned at the same circular arc at 0°. The phantom is rotated for obtaining multi-view data in 40 views. This is equivalent of having a rotation of the antenna; thus a synthetic receiving antenna array rotated with the transmitting antenna is obtained, giving 37×40 complex measurement data points.

In Figures 4.10 and 4.11 the reconstructed real and imaginary permittivity profiles are depicted during the first three iterations, starting from the initial guess of a homogeneous breast without tumor (Figures 4.10 and 4.11 (a)), for both antenna designs. One can see that results are better with the second antenna design, the reconstructed images have fewer artifacts, especially in the imaginary part. The tumor phantom is clearly reconstructed even if some artifacts appear in the imaginary part. These results indicate the importance of choosing an antenna design that enables a minimal incident field model error in the algorithm.

The extended phantom described at the end of section 4.3 is used to to evaluate the systems ability in terms of multi-frequency. As discussed in section 4.4, the main impact of the modification in the 2D-case is assumed to be related to the increased bandwidth of the antenna, therefore, four different frequencies have been considered 950, 1140, 1500 and 2000 MHz. In addition, to comprehend how much of the improvement

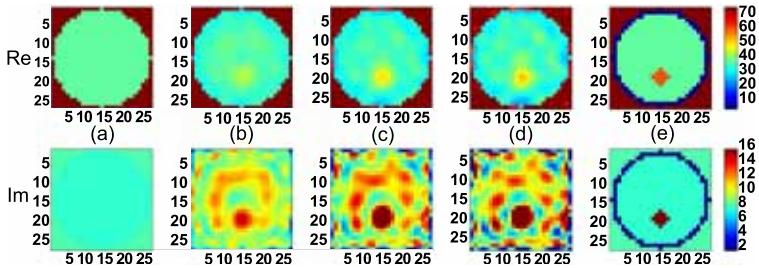

Figure 4.11: Reconstructed real and imaginary permittivity profile of the phantom in Figure 4.4 left using the antenna with the circular ground plane as in Figure 4.5 right. Starting with (a) the initial guess, (b), (c) and (d) iteration 1, 2, 3 respectively, and (e) expected profile. Frequency: 1140 MHz.

in imaging results comes from the upgraded antenna design we compare the reconstructed images using the antenna with circular ground plane without and with the dielectric sleeve. The measurement setup is the same as for the reconstructed scenario in Figures 4.10 and 4.11, except now the receiving antenna scanned around the breast phantom at 91 equidistant points. Measurements along a circular arc are acquired moving 3° between each point from 45° to 315° (moving 270° in total), which gives 91×40 data points when 40 views are performed. The measurement scenario is shown in Figure 4.12.

Comparison of reconstructed permittivity with real and imaginary part (line that goes through the middle of the phantom and the two different smaller PC structures) for the two antennas, the standard monopole and the monopole with the dielectric material on the tip is shown in Figure 4.13. It is hard to draw any conclusion of the real part, but from the imaginary permittivity profile figure one can see that the dielectric monopole is following the expected value better, shown in Figure 4.13. The figures are similar for the other frequencies (not shown).

In Figure 4.14 the reconstructed real and imaginary permittivity profiles are shown for iteration 4 and frequency 950 MHz, individually from real experimental data and simulated data. Starting with the initial guess of a breast without a tumor, deionized water inhomogeneity and PC structure, and the expected permittivity profile in the end. As can be seen in (b) of Figure 4.14, the imaginary permittivity profile from

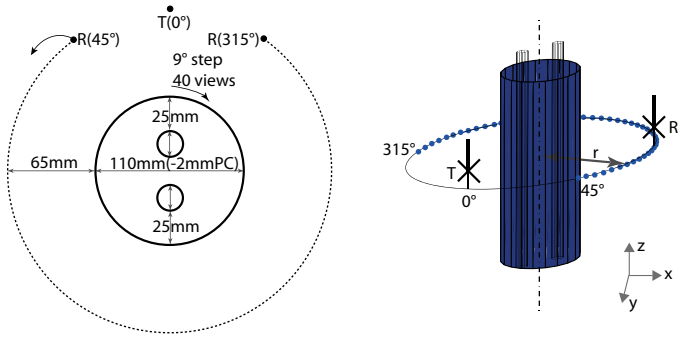

Figure 4.12: The experimental measurement setup in 2D (left) and 3D (right), where R is the receiving antenna, T is the transmitting antenna, r is the radius and the step size between each measurement point is 3°.

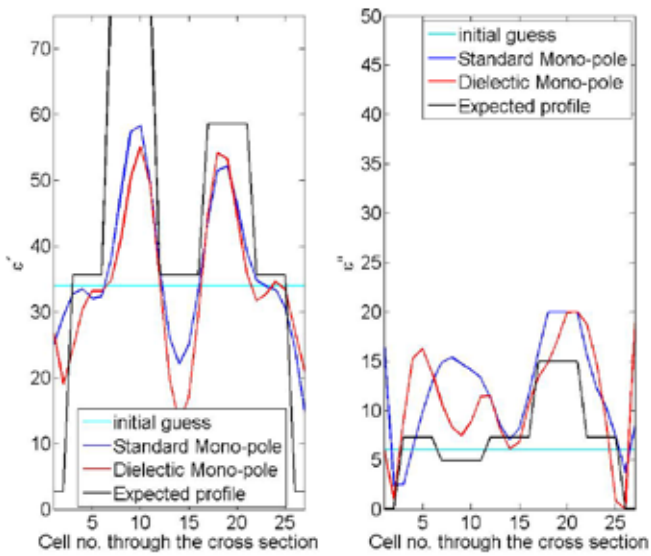

Figure 4.13: Reconstructed real and imaginary permittivity values for a line that goes through the middle of the phantom in Figure 4.4 right. Frequency: 1140 MHz.

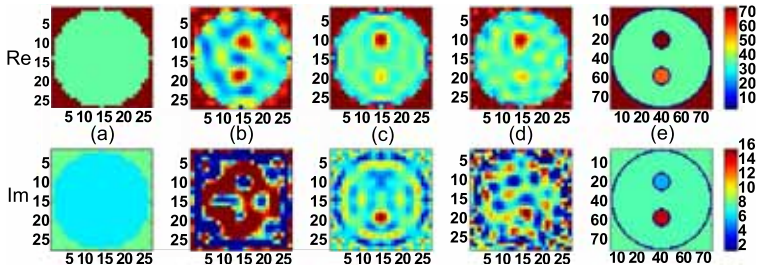

Figure 4.14: Reconstructed real and imaginary permittivity profile of the phantom in Figure 4.4 right using the antenna with the circular ground plane with the dielectric sleeve. Starting with (a) the initial guess, (b) iteration 4, (c) reconstructions from simulation, (d) reconstructions from simulation with SNR 40, and (e) expected profile. Frequency: 950 MHz.

experimental data shows big artifacts, and therefore in (c) and (d) reconstructions from simulation are shown with the plastic material around the smaller objects inside the breast phantom. These results show that even in noiseless simulation data (c) artifacts appears, and the imaginary permittivity profile is completely destroyed with SNR of 40 dB in Figure 4.14 (d). The high contrast in conductivity between the extremely low loss polycarbonate and the tissue simulation liquids cause too strong artifacts in the reconstructed imaginary permittivity profile, even if the PC structure is only 2 mm thick. This confirms that the PC material will affect the reconstructed images particularly in the imaginary part, and thus only the real part will be used for comparison of the results.

In Figure 4.15 the real permittivity profiles are shown for four different frequencies with column I and III representing the antenna without and column II and IV with the dielectric sleeve. The column I and II are the third iteration as in previous case (Figures 4.10 and 4.11), but now even iteration 4 is presented in column III and IV iteration . As can be seen, a better result is obtained after four iterations for the frequency at 2 GHz. Comparing the reconstructed images with the expected profile (Figure 4.15 ((e)), we can see that a better performance is achieved for the antenna with the sleeve on a wider frequency band at 950 MHz and 2000 MHz. In which the tumor and the deionized water inhomogeneity are better reconstructed with less artifacts, while for the frequencies 1140 MHz and 1500 MHz the difference is much smaller. One of the rea-

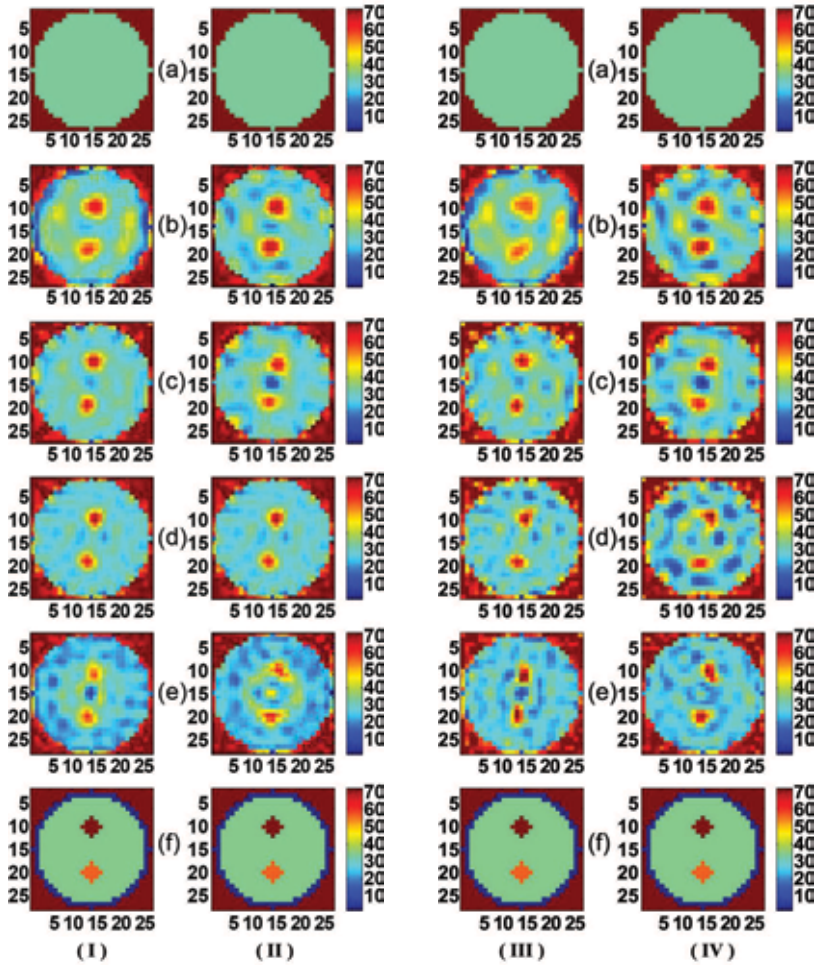

Figure 4.15: Reconstructed real permittivity profile of the phantom in Figure 4.4 right. Starting with (a) the initial guess, (b), (c), (d) and (e) iteration 4 for 950 MHz, 1140 MHz, 1500 MHz and 2000 MHz, respectively, and (f) expected profile. Column I and III, iteration 3 and 4 respectively for the antenna without the dielectric material. Column II and IV, iteration 3 and 4 respectively for the antenna with the dielectric material.

sons for the clutter artifacts in the images is due to the high dielectric contrast between the tubes and the breast tissues. That indicates the importance of designing suitable reference phantoms for validating microwave imaging systems, even if the frequency is relatively low. Other small artifacts are related to pure noise and measurement errors, which are even more important in the case of an object with high losses and relatively low dielectric contrast between the mimicking breast tissue and the tumor and the deionized water filled cylinder. As reported in [81,82] the dielectric contrast between normal breast tissue and tumor tissue might be significantly lower than previous reports [90], [91] requiring a more sensitive MWI system. In our case, the dielectric contrast is approximately 1.6:1 which is pretty low, considering a homogeneous breast tissue with $\varepsilon_r = 35.6$ and a tumor with $\varepsilon_r = 58.6$. The reconstructed images are quite good, and that confirms the system's ability of handling a low-contrast scenario and it could be improved even more by increasing the dynamic range of the acquisition system and introducing more receiving antenna measurement points.

Chapter 5

Applicator Antenna Design for the Measurement System Mamacell

In the framework of our forthcoming work, with the measurement system called Mamacell, on designing and implementing a smaller and more adapted prototype MWI system; that could be used in clinical investigations for breast cancer detection, the need for new antenna applicator is envisaged. The main idea with the Mamacell design is to develop a robot based measurement system, similar to our MWI system described in Chapter 4 but in much smaller scale, for positioning of the measurement antennas. This is a compact device for only two antennas (sensors), one transmits and one receives, that are placed at different locations directly on the imaging object. The positioning device is a small, two arm robot system that will position the antennas with high precision on the imaging object in any point, in the measurement domain, approximately $25\times25\times25$ cm.

Most of the experimental MWI system setups use a coupling medium to couple the microwave energy into the body. The coupling medium introduces losses, which attenuates the imaging energy and using a system without coupling medium would increase the possible dynamic range al-

lowing reliable acquisition of the weak scattered field. The idea with the robot system (Mamacell) is to place the antennas directly on the breast and, therefore, eliminate the need of a coupling medium for energy coupling reasons.

The main focus of our research group, as stated in Chapter 2, is to investigate the usage of microwaves as a possible imaging method in biomedicine. This robot prototype system is supposed to be used to image the human breast and thus place the antennas directly on the body. Hence, the antennas need to be compact for easy placement on and around the breast surface. The realization of such an imaging system requires some research to be performed to answer a couple of questions. One question that arises when considering antenna design, such as an applicator antenna, to be placed in direct contact or in close proximity with the imaged object. How can microwave sensors/applicators be constructed to efficiently couple energy into the imaging object? This question is tightly connected to RQ3 in the Chapter Problem Formulation, and is one of the main research challenges of this part of the thesis. For this purpose the main constraints and design requirements remain in a narrow lobe of the antenna, very small near-field effects, and small size. This is challenging because of the complex structure of the imaged object's (biological tissues) dielectric properties. Antennas placed on the body are being designed for maximum energy coupling into the body is a relatively new approach in MWI systems but has similarities with antennas used for hyperthermia treatment or food processing. Various antenna design has been considered for near-field microwave imaging and especially for biomedical applications, e.g. the miniaturised bow-tie antenna [92], the TEM horn antenna [93], a cross Vivaldi [94] and a balanced antipodal Vivaldi antena [95, 96], the stacked-patch and wide slot antennas [97], and an applicator design based on a dielectric loaded Vivaldi element [98, 99].

5.1 General - Basic Constraints and Performance Goals

In the Mamacell project, small antennas are needed despite the operating frequency range being 1 to 3 GHz. A possibility is then to use quarterwave or shorter pin monopole antennas with or without a ground plane similar to those explained in section 4.4. Whereas the monopole

antenna has the advantages of being easily modeled and simple manufacturing, and on the other hand disadvantages of omnidirectional radiation pattern. Having in mind that they should be in direct contact with the imaged body, thus increasing influences from the surroundings away from it, and the omni-directivity also causes power losses by waste in wrong directions. Another disadvantage is the very strong non-radiating near-fields, which results in a system sensitivity to minor inhomogeneities close to it, and also in a power loss resulting in a reduction of the received signal strength between the transmitting and receiving antennas.

The candidate for our new system is the end-fire contacting antenna. This antenna design is more complicated to manufacture than the monopole. However, there are many advantages with such antenna applicator: a) a lobe pattern which is made narrower than from a TE_{10} waveguide into free space; b) very small near-field effects allowing direct contact and by that a further increased use of the available power as well as improved reception; c) by the smaller lobes also a reduced influence by the surroundings; d) a polarized pattern allowing quite interesting increases in discrimination of tumors by using particular diffraction effects caused by it. A disadvantage may be issues related to the precise descriptive equations for its radiation pattern, i.e. modeling. However, simplified non-physical antenna models may be employed in the computations, once their validity has been established, by retro-modelling.

5.1.1 The Basic Constraints and Design Requirements

The manufacturing aspects are a compromise between the microwave engineering and fabrication possibilities. The idea is to have the antenna aperture, opening surface, lightly contacting a human female breast or an intermediate jelly like material, with permittivity higher than about 6 for avoiding breast deformation and reducing field evanescence. The total aperture area diameter should be less than about 15 mm and the frequency range of useful operation from 1 to 3 GHz.

5.1.2 The Most Desirable Performance Goals

The most desirable performance goals of the antenna are matching in the 1.5 to 3 GHz band with less than 3 dB, i.e. 50% of power loss corresponding to a reflection factor less than 0.7. The narrowness of the antenna lobe should be the best possible in both perpendicular (x, y)

planes along the direction (z) of propagation. In particular, propagation along the breast surface should be low. The performance of the antenna should have as low sensitivity as possible to the detailed structure of contacting region and of imperfect contacting over the whole aperture area, i.e. a short Fresnel region.

5.2 Design Strategies

The applicator is designed in separate parts which simplify the work and also the optimization will more clearly indicate hurdles and allow closer analysis towards improved synthesis. To achieve the design requirements and desirable performance, the applicator is divided in the following separate parts, from the front end:

1. Protective cover of the antenna aperture (section 5.1.1), also having an optimized function of minimizing the system sensitivity to variations of contacting tissue type and undesired sideways propagation (section 5.1.2).

2. A mode and field transmission section between the coaxial transition section and the aperture opening feed. In this part the field pattern is shaped to become more TEM-like, thus resulting in a minimization of the near-field. There are also compensating matching properties, reducing the overall mechanical complexity and size.

3. The transition from a coaxial line input to the transmission section, with the coaxial center conductor going all the way through the waveguide for practical manufacturing reasons.

4. The coaxial transition to the waveguide and its feed section, for achieving frequency independence of matching and importantly a narrow lobe.

5.3 The Transmission Section and Antenna Feed Adaptability

A coaxial line end as antenna is a short electric dipole having E and H fields such that the propagation away from it is radially outwards,

along the ground plane, therefore direct connection of a coaxial line section to the aperture without mode transformation is not possible. The applicator to be designed must have the propagation maximum straight outwards from the aperture. The simplest transmission line modes providing this are the circular TE_{11} and the rectangular TE_{10} waveguide modes. Therefore, the mode in the transmission section should be one of those, for facilitating a direct transition to the antenna section.

5.3.1 Frequency Cutoff and Bandwidth Considerations

The lowest usable frequency (1 GHz) implies that the wide *(a)* dimension of a rectangular air-filled waveguide must be at least 150 mm (i.e. half the free space wavelength). Filling it with a dielectric of a permittivity $\varepsilon' = 25$ reduces this by a factor of 5, to 30 mm. However, the small cross section of the aperture shall be even smaller according to the design requirements around about 15 mm. The factors that are considered for the choice of the dielectric with which the waveguide must be filled:

- The permittivity of the load which the aperture is contacting should have a similar ε', which will minimize the mismatching. The breast and related tissue ε' is set to 20, for the purpose of system optimization in this respect.
- According to the performance goal above (section 5.1.2) a short Fresnel region is the second factor to consider: a higher equivalent ε' of the aperture region will result in a faster spatial evanescence of the wave energy in a low permittivity (air)gap between the aperture and the tissue. This is a negative factor to consider.
- Commercially available pourable sand type solid dielectrics can have ε' up to about 17. For higher ε' there are only two realistic choices of commercially high purity ceramic dielectrics: ZrO_2 with $\varepsilon' = 35$ and TiO_2 with $\varepsilon' = 90$.
- Having a short Fresnel region in mind investigations should first be made with ZrO_2, together with a filling of the $\varepsilon' = 17$ material.

Even with a complete filling with $\varepsilon' = 35$, the 1 GHz cutoff rectangular TE_{10} waveguide gets a dimension of more than 25 mm. Therefore, a ridged waveguide becomes necessary. Such waveguides have a cross

section where there are inwards-going metal parts in a centre portion of one or both a sides. This leads to an increased capacitance, while the inductance remains relatively unchanged. The result is a lower cutoff frequency. Ridged waveguides have two other advantages in this case:

- Higher order waveguide modes do not go down in cutoff frequency as does the normal mode TE_{10}, since they do not have their E field concentrated to only the center *a/2* part. This means that it is possible to have no other propagating mode up to 3 GHz or even higher, which in turn results in less change of the lobe pattern with frequency.
- A transition from coaxial line to the TE_{10} mode in the ridged waveguide becomes less complicated with a ceramic body all the way between the ridges, since good contacting is easier to accomplish in a small diameter (the drilled) hole which is needed for obtaining impedance matching than with pourable sand type solid dielectrics.

The permittivity of the ceramic ridge insert and that of the filler of the remainder has to be balanced against the properties of the contacting (breast) substance, for the best compromise transmission and insensitivity to air-gaps/deformation. The ridge permittivity should then be somewhat higher than that of the aperture contacting region, and the remaining filler permittivity be about half of the ridge.

The cross section of the chosen geometry is shown in Figure Figure 5.1. The two lowest cutoff frequencies are 998 MHz (TE_{10}) and 3831 MHz (TE_{20}), basically independently of any working excitation field. They are computed with the commercially available modeling software Quickwave©. A very important advantage of the ridged waveguide design is the fact that only the desired mode can occur in the transmission section for any frequency between the two.

5.4 The Antenna Part

5.4.1 Properties of the Transmission Line Cross Section As Antenna

The images in Figure 5.2 are with a large metal ground plane at the end of the transmission line shown in Figure 5.1, and directly contact-

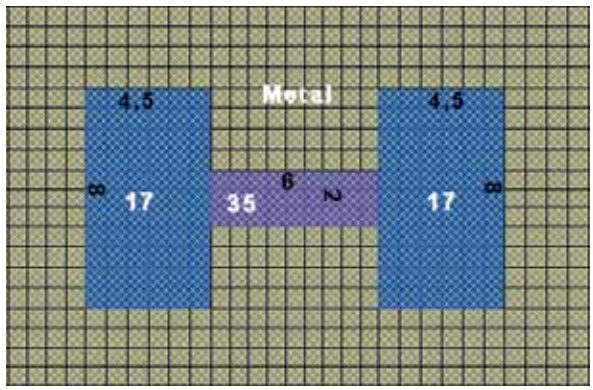

Figure 5.1: The cross section of the TE line. The white numbers represents the choice of dielectric material, where the ceramic ridge is set to $\varepsilon' = 35$ (ZrO_2) and the reaming filler $\varepsilon' = 17$ (sand or acetone). The black numbers are the dimensions of the ridged waveguide in millimetres.

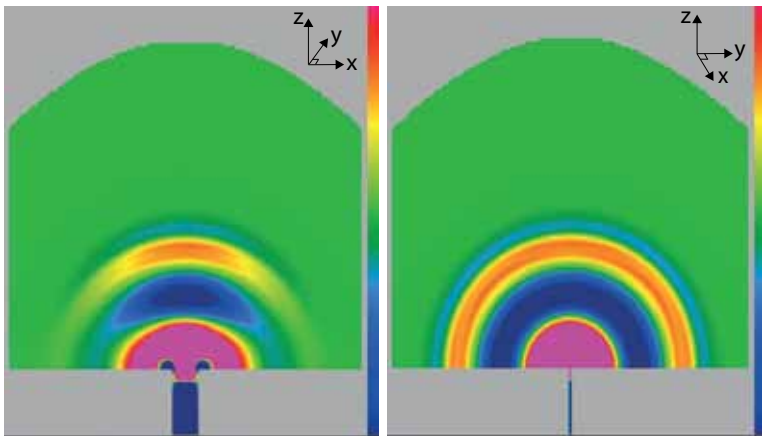

Figure 5.2: The momentaneous x-directed magnetic field in the x-directed central cross section, i.e. in the plane of the waveguide a dimension (left image), and in the y-directed central cross section (right image), at frequency 1.22 GHz.

ing simple simulated homogeneous breast tissue with $\varepsilon' = 20$ and very low constant equivalent conductivity $\sigma = 0.011$. The reason for choosing the low value of $\sigma = 0.011$, is that the undamped radiation lobe and impedance matching are of interest here, where the later is quite independent of ε''. In this test case, wave reflections at any air boundaries are unwanted, since the radiation lobe is of interest. Therefore, the metal plane is large 200 mm x 200 mm, and with the antenna centred. The load/breast height is also 200 mm. The FDTD methods suffer from issues related to wave propagation into infinity: special absorbing surfaces must be used and the approximations for these are complicated, in particular along edges and in corners. Furthermore, the so called MUR approximation used here works less well when the medium is not air. Therefore, the method of avoiding outer boundary reflections in this case is to use such a large load/breast volume that many periods of the propagation into it occur at the antenna aperture before the fields reach any outer boundary. In particular the x-directed magnetic field dominates and can therefore be used for the analysis. It is seen in the left Figure 5.2 that there is a significant upwards-directed lobe, the ratio between the amplitude in the z and x directions is 11. However, in the central y plane (right image) the situation is very different where the ratio between the amplitude in the z and y directions is almost exactly unity.

5.4.2 Antenna Design Reasoning

Once the wave propagation approach is chosen, the function of the transmission line (described in section 5.3) as antenna and shown in Figure 5.2 needs to be explained in terms of fields and waves, in some analogy to what is described in the paper [96] as director. But its function is not related to geometric optics. Comparing Figure 5.1 with the result in the left Figure 5.2 indicates the following:

- The group speed of the wave energy is lower in the central section due to the higher $\varepsilon' = 35$ there than outside it (having $\varepsilon' = 17$). The central retardation results in the curvature radius of the x-directed H field to increase when it leaves the transmission section, and the same applies to the phase of the y-directed E field. The wavefront outside the aperture thus becomes more plane like.

- This distortion of the fields is simple and occurs over a very short

distance, also in relation to the transmission line wavelength. As a consequence, the spherical or cylindrical propagation begins almost immediately in the aperture region.

The following hypotheses can now be made:

1. By introducing a less abrupt termination end of the high permittivity centre part in an antenna section (i.e. no longer just the end of the transmission section), it is possible to further "sharpen" the lobe in the x-directed cross section.

2. There is no centre part with higher ε' surrounded by parts with lower ε' in the y-directed cross section, but this can be accomplished by extending the b dimension in the antenna section.

The realization of the first hypothesis results in what is currently called a "projectile ceramic director", and that of the second hypothesis of a E-plane horn section (with director), which is a sectoral horn flared in the direction of the E field and containing a higher ε' director. An example of the above mentioned antenna design can be found in Paper E (chapter V, section C).

5.4.3 The Final Proposed Antenna Design

For the final applicator antenna design the commercially available dielectric zirconium oxide (ZrO_2) was chosen for the ceramic ridge insert with $\varepsilon' = 35$ and a commercially available filler were set to $\varepsilon' = 17$. The design is shown in Figure Figure 5.3. It is seen that the ZrO_2 ceramic becomes symmetrically pyramidal. This is over 15 mm axially, and the top dimension is 2×2 mm, Figure 5.3.

As stated before, the manufacturing aspects are a compromise between the microwave engineering and fabrication possibilities. The applicator is as small as it can reasonably be made in terms of fabrication. The final design and fabricated antenna is shown in Figure 5.4.

A modeling scenario is arranged in a way that the antenna is contacting a breast tissue with a permittivity value of $\varepsilon' = 25$ and conductivity $\sigma = 1$. In-between the antenna and the breast tissue there is a 2 mm thick skin and fat layer with $\varepsilon' = 5$ and $\sigma = 0$. The momentaneous magnetic H_x-field is shown in Figure 5.5 using a mode template as on the right in Figure 5.3, but the antenna applicator is as in Figure 5.4. The H_x-field strongly dominates in the breast dielectric, and a close study

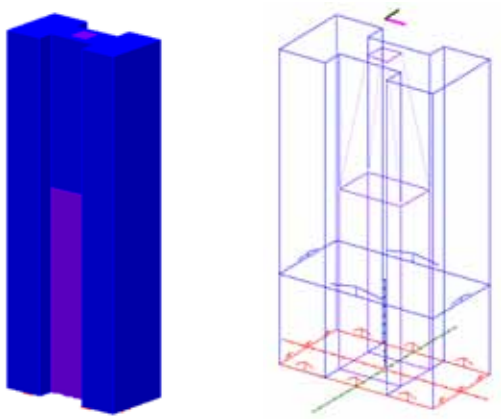

Figure 5.3: Waveguide applicator antenna in opaque (left) and transparent 3D (right)with an underlying transmission line with a so called mode template (i.e. well impedance matched) excitation.

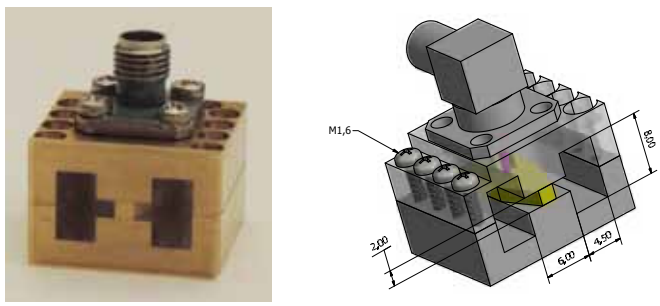

Figure 5.4: The final antenna applicator design showing the overall size of the antenna (right); and a photo of the manufactured antenna (left); dimensions in mm.

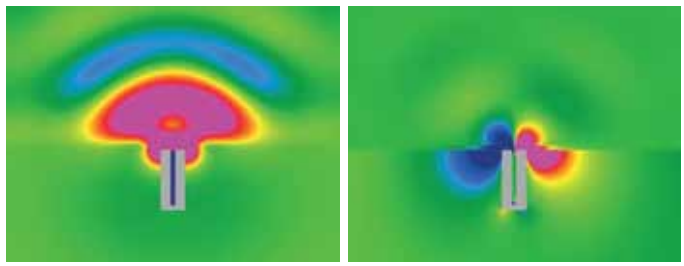

Figure 5.5: The momentaneous H_x-field under stationary condition in the vertical x plane (left). The image size is truncated to ±70 mm in y-directions and totally 110 mm in z-directions, of a much larger scenario. The right image is the momentaneous E_z field intensity. Frequency: 1.5 GHz.

reveals that there is a propagating spherical wave already about 15 mm from the antenna opening.

The z-directed electric field intensity, all data equal as in previous case for the H_x-field, is shown in the right Figure 5.5. The E_z field is that which can create Zennek waves, but it is rather poorly field-matched and thus mainly a standing wave. Therefore, means to reduce that field should be sought for. The first order method of reducing disturbances by direct and Zennek wave propagation between adjacent antennas is by orienting them 90° rotated.

The impedance matching is shown in Figure 5.6 using a mode template as on the right in Figure 5.3, but the antenna applicator is as in Figure 5.4. The modeling scenario is the same as in the previous case of Figures 5.5. The mode template does not work for frequencies below the cut-off, which is 998 MHz for the transmission in the modeled antenna. It is seen that the reflection factor has a small transient at the waveguide cut-off. It is also seen that the variation with frequency is quite undisturbed by resonance effects. Hence, the system is shown to be inherently non-resonant.

A simple 50 Ω coaxial feed with 1×1 mm cross section inner conductor throughout the ZrO_2 section is applied 6 mm from the end shorting wall. The resulting reflection factor from 0.7 GHz to 4 GHz, with a matched mode template at the other end of the waveguide, is shown in Figure 5.7. It is seen that a reasonably good system matching is achievable, and the

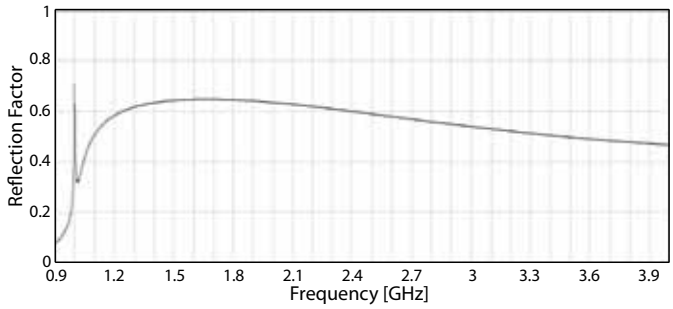

Figure 5.6: The impedance matching (reflection factor amplitude) of the antenna applicator as a function of frequency (0.9...4 GHz), using a mode template matched to the transmission line input end, and loaded at the opening.

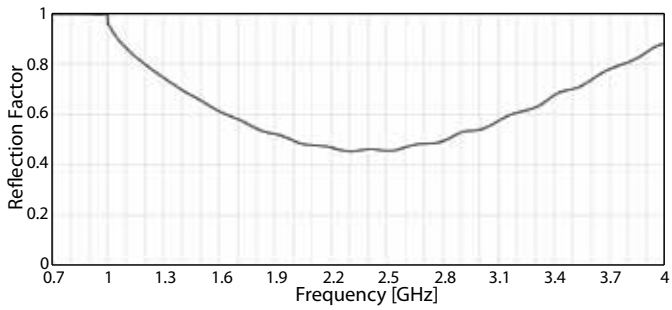

Figure 5.7: The reflection factor from 0.7 to 4 GHz for the scenario with the antenna fed by the coaxial transition and having a matched mode template at the other end.

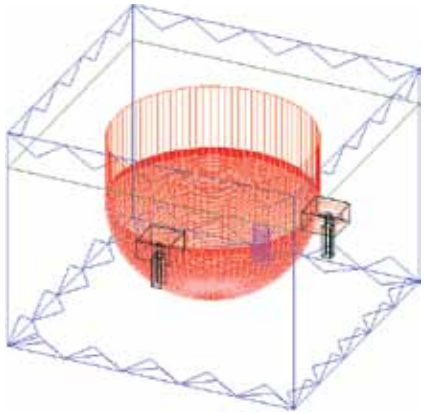

Figure 5.8: A ceramic Eccostock® breast model with $\varepsilon' = 25$ and $\sigma = 0.0034$, and a tumor with data $\varepsilon' = 20$ and $\sigma = 1.3$.

reflection factor is below 0.7 in the 1.5 to 3 GHz frequency band, which fulfils one of the desired performance goals according to subsection 5.1.2.

5.5 Modeling with the Antenna

Modeling is performed in order to analyze the field patterns and get an understanding of the important factors to consider for improved tomography results. A full arrangement of the modeling scenario is shown in Figure 5.8, where a ceramic breast model with rounded breast surfaces are surrounded by air. Dielectric breast data are set to $\varepsilon' = 25$ and $\sigma = 0.0034$, according to the real fabricated Eccostock® breast model built of a dielectric material called HiK 25 [100]. The size of the breast Model is 100 mm diameter short cylindrical piece with a hemisphere attached to it in air. A tumor is displaced by 25 mm in the $+x$ direction from the breast *(z)* axis (not the same reference as the propagation direction in the antennas) and parallel to that; bottom of tumor 20 mm above the lower end of the breast. Above the breast there is a 20 mm high layer of methanol, with set permittivity of 20 and conductivity 1.3. There is a MUR-approximation absorbing plane at all scenario sides.

The horizontal plane of the contacting antenna opening are shown in the images in Figure Figure 5.9. In all depicted field images the 6 o'clock

antenna is energized, and all images are without the tumor present. This is in order to check the imaging field symmetry and any disturbances by the receiving antenna. The (a) image is of the momentaneous x-directed electric field at frequency 1.2 GHz (green = 0), i.e. the left-right-directed in the image, with a set amplitude for the red/magenta (and light/dark blue) of 0.01 (relative scale). The (b) image is all the same, except the electric field is now the y-directed (i.e. up/down in the paper plane). In (c) the z-directed field at 1.2 GHz is presented, and with a set amplitude for the colors 5 times higher than in previous images (a) and (b). Many phenomena can now be observed:

- There is very little leakage out of the breast of the dominating E_z field.
- There is a significant narrow lobe of the E_z field.
- The E_x and E_y fields are characteristically 5 times weaker (i.e. each has 4% energy density compared with the z-directed).
- An external standing surface wave (Zennek wave) is the dominant phenomenon of the E_x and E_y. Both have a dipolar configuration displaced by 90°, so the mode is of the external TE_2 type.

The phenomena are similar at 2 GHz, as shown in Figure 5.9 (d) and (e), where the (d) image is the x-directed field and the (e) image is the z-directed field. It is to be noted that the amplitude scaling is now ten times lager in the E_z image. Again, the lobe effect is seen, now even more clearly. Also the surface (Zennek) wave pattern is now very clear. It should be noted that Zennek waves have a very long so called decay distance along the surface, i.e. their energy content is damped to 37% over a distance which is in this case several meters. What then happens is that a standing wave pattern, which may be partially resonant, is created. Reduction of Zennek waves is therefore an important task.

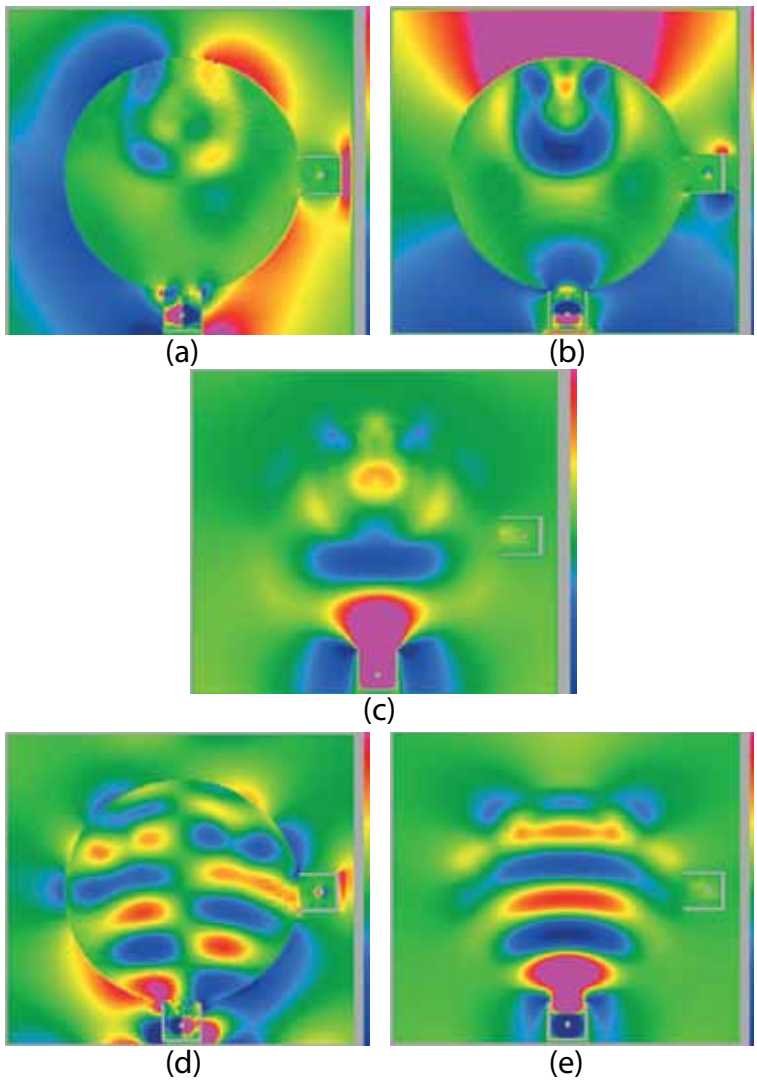

Figure 5.9: The momentaneous electric field where, (a) x-directed, (b) y-directed, (c) z-directed, (d) x-directed and (e) z-directed.

Chapter 6

Contribution

This chapter is divided into two parts. The first part is a summary of the research work throughout Paper A-E in relation to the research questions formulated in Chapter 2 will be discussed with the help of the contributions in the included papers. The second part of the chapter Paper A-E is presented in short summary with the specific scientific contribution and the author's contribution for each paper.

6.1 Summary of The Research Work throughout Paper A-E

The first step in the research work, after literature studies and putting up the ideas, is the design process, where we in Paper A present and validate a flexible robot controlled data acquisition system for the main propose of microwave imaging. Research challenges in this study are connected to RQ 1. The receiving antenna positioning enables accurate investigations of different synthetic antenna array geometries without introducing coupling effects between multiple antenna elements in the system design stage. Also, a wideband system for suitable frequency determinations is achieved with a rapid data acquisition time. This system can be seen as a platform for investigations of scattering fields around an object and as a platform for achieving the goal to quantitatively reconstruct it.

In Paper B the research challenges are associated with RQ 2, and the next phase of the research work are related to the characterization

of dielectric material properties and phantom development. In order to create phantoms mimicking human breast tissues a feasibility study was done of a so called reentrant cavity, a sort of a cylindrical cavity. The first jelly based phantom created, based on 1.2 propylene glycol, showed to be inappropriate for image reconstruction and was therefore discarded. On the other hand, the cavity method was confirmed to be an accurate method for permittivity measurements, however; a decision was taken to move on with the open ended coaxial probe for convenience reasons. A new phantom design using Triton X-100 and water mixtures was created and proved to be a good candidate for the purpose of image reconstruction.

Paper C is addressing model errors and their impact on the incident field model. In this study, we are pointing out the importance of choosing the antenna design that minimizes the errors between the measured and computed fields. Herein we are starting to scratch on the surface of RQ 3, considering improvements of the simple monopole antenna. The MWI system was at the same time validated in terms of quantitative image reconstructions for the first time.

In Paper D, a complete data acquisition prototype system able to examine biological mimicking targets for quantitative microwave imaging is presented. The system is upgraded from previous Papers A-C in terms of broadband antennas, permittivity estimation of the background medium, positioning of the rotational axis and finally quantitative image reconstructions of an upgraded breast phantom. In this paper, we are dealing with all three research questions simultaneously reaching in a certain sense the main objective of the thesis.

At this stage of the research project, the decision within the research group at MDH was to move further and build a robotic breast imaging prototype for clinical test on real patients, in that sense moving towards a "real" biomedical application. The realization of such an imaging system requires some research to be performed to answer a couple of questions. The first step was to extend the RQ 3 regarding the question that arises when considering antenna design, such as an applicator antenna, to be placed in direct contact with or in close proximity of the imaged object. For this reason a new antenna applicator is envisaged and introduced in Paper E. The main constraints and design requirements remain in a narrow lobe of the antenna, very small near-field effects, and small size. This is challenging because of the complex structure of the imaged object's(biological tissues) dielectric properties.

The main contributions of this research work are the results from a robotic measuring microwave imaging system together with the designed novel applicator for near filed microwave imaging. A successful attempt is presented in the form of quantitative image reconstruction of inhomogeneous objects by using experimental data from the flexible microwave imaging system. The properties of different monopole antennas are investigated, where a model of the incident field together with the permittivity measurement of the background medium are presented. Also, the extended breast phantom with the cavity permittivity measurement can have an impact on the community, as a simple realization of a breast and the experience of using the resonant cavity method for finding the dielectric properties for the breast mimicking materials. The contribution of the antenna design, in terms of an applicator, for near filed microwave, imaging is a candidate for MWI systems where the antenna is to be placed on the surface in direct contact with the breast tissue.

6.2 Contribution of Included Papers

This section will present each paper with a short summary following scientific contribution and the author's contribution to the included papers.

6.2.1 Paper A

Title **Robot Controlled Data Acquisition System for Microwave Imaging**

Authors Petrović, Nikola. Henriksson, Tommy. Joachimowicz, Nadine. Otterskog, Magnus.

Source Conference on Antennas and Propagation (EuCAP 2009), p 3356-3360, VDE Verlag GMBH, Berlin.

Publication type Conference Publications

Summary

In this paper, an experimental prototype of a robot controlled data acquisition system for microwave imaging is presented, where the transmitting and receiving antennas are immersed in a water-tank. The scattered field from the object under test is acquired by using the robot and scanning a single receiving antenna in cylindrical or half spherical coordinates, while the transmitting antenna is fixed at one position with possibilities to be manually moved to different positions. Careful design and construction of the system has given accurate measurements of incident and total field. A validation of the robot system is performed by comparing measured and computed data for a sunflower oil object. A good symmetry of the measured data is achieved with a symmetric object configuration, and potentially low error between measured and computed scattered field gives promising condition for future image reconstruction studies.

Contribution

A validation of an experimental setup of a flexible data acquisition system for empirical measurements that can be used to evaluate different measurement scenarios, with high accuracy, for the purpose of microwave imaging. A simple antenna design with a flexible synthetic array antenna positioning.

Author's contribution

Main author of this paper and a major part of the idea of designing the MWI system. Hardware development of measurement platform including design and testing. Performed measurements and had role in the experimental validation.

6.2.2 Paper B

Title **Permittivity Measurements with a Resonant Cavity to Develop Human Tissue Phantoms for Microwave Imaging**

Authors Petrović, Nikola. Otterskog, Magnus.

Source The 8th International Conference on Electromagnetic Wave Interaction with Water and Moist Substances, ISEMA 2009, Helsinki, Finland, 2009

Publication type Conference Publications

Short summary

In order to create human tissue phantoms for a microwave imaging system, a method to determine the complex permittivity is needed. For this reason a cavity perturbation method has been analyzed and used to perform measurements characterizing the complex permittivity of different fluid mixtures. Results show good agreement on single frequency between the measurement with the reentrant cavity and references. However the complex part of the final material mixture mimicking human tissue are higher than expected, which makes 1.2-propylene glycol inappropriate as a human tissue phantom material. The cavity perturbation method is still a suitable method for measuring liquids and with more work it might even be reliable for gel-based materials. Triton X-100 and water mixture are used at the present as breast phantom materials and initial studies have shown promising results.

Contribution

A feasibility study of a method to determine the complex permittivity using a resonant (reentrant) cavity with measurements on fluids and materials simulating some biological tissues.

Author's contribution

The first author of the paper and responsible for the cavity measurement method. Also created the phantom to be used for collecting multi incidence set of data from it, by the robot based acquisition system in order to quantitatively reconstruct the phantom.

6.2.3 Paper C

Title **Antenna Modeling Issues in Quantitative Image Reconstruction Using a Flexible Microwave Tomography System**

Authors Petrović, Nikola. Henriksson, Tommy. Otterskog, Magnus.

Source PIERS Progress In Electromagnetics Research Symposium, Cambridge, USA, Volume: 6, NO: 5 Page(s): 450 - 454 , 2010

Publication type Conference Publications

Short summary

In this paper two different monopole antenna designs have been validated in a flexible microwave tomography system. The results show how the selection of antenna design impacts the error between the measured incident field and the numerical incident field model. Herein, the radiated field from the antenna is modeled as a vertical polarized cylindrical wave, in the numerical incident field model of the algorithm. By comparing the reconstructed images of a simple breast phantom it was shown how the quantitative image is affected by this model error. Using an antenna design that minimizes the error between the model and the measured values leads to a better reconstruction of the object. This confirms the importance of minimizing the model error inside the object region. In this paper the first reconstructed images by the Newton Kantorovich algorithm of a breast phantom was shown and that confirms the microwave system's ability to produce quantitative images.

Contribution

Validation of the system in terms of comparison of two different monopole antenna designs with the incident field model in both amplitude and

phase, using data conducted by the flexible MWI system. We have shown that the selection of antenna design impacts the error between the measured incident field and the numerical incident field model by comparing image reconstructions.

Author's contribution

Experimental setup with measurements, model extraction and wrote most of the paper.

6.2.4 Paper D

Title **A Novel Flexible Data Acquisition System for Quantitative Microwave Imaging**

Authors Petrović, Nikola. Henriksson, Tommy. Ekström, Mikael. Otterskog, Magnus.

Source Submitted to IEEE Transactions on Instrumentation and Measurement

Publication type Journals and Magazines

Short summary

This work presents a novel platform of a flexible measurement system validated through examination of quantitative microwave imaging from experimental data of a low-contrast breast phantom. An improved vertical polarized monopole antenna is used, attached to a robot axis possible to move the antenna in different synthetic array geometries around the breast phantom. The antenna is designed with a dielectric sleeve covering the protruding tip of the antenna, enabling broadband measurement with the MWI system. In this study, the breast phantom is placed in water, as a background medium, and the receiving antenna is scanning around the phantom in a cylindrical geometry measuring the scattered field component. In addition measurements are done for estimating the background complex permittivity using the existing antennas in the system, and a developed method for positioning the rotational axis utilizing an ultrasonic sensor. These features together with the enhanced monopole antenna design, to produce good reconstructed images minimizing the model errors between measured and computed

values, making the MWI system more advanced and effective. By using the experimental experience gained from this work and designing new antennas (sensor/applicator) the research group at MDH aims to build a breast robot prototype, for clinical tests on real breast cancer patients, capable of imaging in 3D.

Scientific contribution

Complete hardware platform for quantitative microwave image reconstruction. An upgraded experimental setup with possibilities of measuring the complex permittivity of the background medium and also an ultrasonic positioning system for the rotational axis. In addition an enhanced antenna design have been used for image reconstruction for different frequencies.

Author's contribution

Hardware development including antenna design and testing. Calibration including incident field model, permittivity estimation and positioning. Validation of the complete MWI system. Furthermore prepared most of the manuscript.

6.2.5 Paper E

Title **Antenna Applicator Design for Microwave Imaging of the Interior of Human Breasts**

Authors Petrović, Nikola. Otterskog, Magnus. Risman, Per Olov.

Source Submitted to IOP Science, Journal of Physics D: Applied Physics, April 2014

Publication type Journals and Magazines

Short summary

In this paper we introduce a waveguide antenna applicator design intended to be placed on the surface or in close proximity to a human breast for imaging purposes. Hence, the antenna needs to be compact for easy placement. The design process is carefully carried out dividing

the antenna applicator into separate parts, allowing closer analysis towards improved synthesis. A mode applicator antenna was concluded to be necessary, employing a TE_{10} mode type with minimized near-field and surface (Zennek) wave excitation. Numerical simulations have been used throughout and shows that the proposed ridged waveguide antenna is capable of fulfilling the design requirements and the performance goals. Modeling has been carried out using a scenario with a simple breast model and confirms the applicator's capability.

Scientific contribution

A novel antenna applicator for near-field microwave imaging of the breast has been presented and fabricated. Our proposed applicator concept provide a small antenna with enhanced plane wave propagation in the breast, at the same time reducing near-field effects at the antenna aperture as well as excitation of breast surface waves. The compact design allows good contacting without deformation of the breast and an easy multiple positioning. An improved lobe pattern by using a ridge waveguide with two dielectrics providing a quite directive lobe pattern.

Author's contribution

The first author of the manuscript with the idea behind the paper. Together with Risman and Otterskog developed the antenna applicator through discussions and simulations.

Chapter 7

Conclusions and Future Work

This chapter will summarize the work presented in this doctoral thesis. The continuation and future work within this topic will conclude the discussion and thesis.

7.1 Conclusions

This thesis deals with the issues related to microwave imaging towards biomedical applications with the emphasizes on breast imaging. The problem related to measurement systems with associated tools and antenna design for microwave imaging is addressed in Chapter 2, whereas the discussion and scientific contribution of the included papers are presented in Chapter 6.

The problem formulation is divided into three research questions, and these are derived from the main formulation of the general research problem that lay the ground for the work presented. The aim is of course to give the complete answer and solution for all of the presented research questions in chapter 2, and reach the main objective, which we in a way are fulfilling. However, our view is that the solutions in this thesis are not giving the complete answers they have rather opened up for a new goal to work towards, namely the new measurement system called Mamacell.

The work presented in this thesis was focused on a measurement system for quantitative microwave imaging and an antenna applicator designed for a new system planned to be built in the near future. A designed flexible measurement system, validated through examination of microwave imaging from experimental data of a low-contrast multi-target breast phantom, shows a successful solution in the form of 2D quantitative image reconstruction. These results demonstrate the measurement system's ability to obtain high quality scattering data for quantitative image reconstruction for biomedical applications. In this measurement scenario, the breast phantom is placed in water, as a background medium, and the robot is generating a synthetic antenna array around the phantom in cylindrical geometry measuring the scattered field component using different monopole antenna designs. In addition measurements are done for estimating the background complex permittivity using the existing antennas in the system, and a developed method for positioning the rotational axis utilizing an ultrasonic sensor. These features together with the enhanced monopole antenna design reduces the model errors between measured and computed data, which also improves reconstructed images and making the microwave imaging system more complete and effective.

By using a robot controlled measurement system we are minimizing the positioning error of the system since the accuracy is very high. The robot's degree of freedom allowing us to use different geometries forming different synthetic arrays for the receiving antenna. Such a flexible receiving antenna enables a selectable number of measurement points without introducing coupling effects between multiple antennas in the system.

A monopole antenna design was utilized in the MWI system and improved in two steps. The first upgrade was designed to fit the numerical incident field model minimizing the error between the measured values and the model. Comparison of the reconstructed images of a breast phantom shown the impact of model errors on the quantitative images, where the antenna design that minimizes the error leads to a better reconstruction. The second modification of the monopole antenna demonstrates increased bandwidth, for this reason four different frequencies were considered and compared through image reconstruction. Conclusion is that the antenna with the dielectric sleeve on the protruding tip performs better on a wider frequency band, i.e. at 950 MHz and 2000 MHz in a 2D-case.

Whereas the monopole antenna has the advantages of being easily modeled and simple to manufacture, on the other hand they are not suitable for placement in direct contact or in close proximity with the breast object. The disadvantages in this case are the omnidirectional radiation pattern causing power losses by waste in wrong directions, and also increasing influences from the surroundings away from the breast. Another disadvantage is the very strong non-radiating near-fields, which results in a system sensitivity to minor inhomogeneities close to it, and also in a power loss resulting in a reduction of the received signal strength between the transmitting and receiving antennas. This leads us to design and develop a new antenna for the measurement system called Mamacell.

A very significant majority of antennas intended for the purposes of microwave imaging are designed with the background of communication antenna design. This then includes quite large horn types antennas as well as small patch antennas, the latter then designed with wideband multi-pole modes for achieving broadband functionality. These do not present any specific considerations of disturbing modes and fields.

The starting point for our antenna applicator design was to enhance the desired plane wave type propagation in the breast, at the same time reducing near-fields at the antenna aperture as well as excitation of breast surface waves. A further goal was to reduce the overall size of the antenna providing good contacting without breast deformation and for easy multiple positioning.

So far the work shows promising results and will be followed up with further surface wave reduction, and of course with imaging experiments and computations.

7.2 Future Work

Directions of future works include continuation of the work presented in Chapter 5, i.e. empirical measurements with the objective to further explore the applicator antenna performance. Future works include also finishing the fabrication of a new breast robot measurement system called Mamacell, able to put the antennas (one transmitter and one receiver) in direct contact with the breast surfaces in different half spherical scenarios. As an initial antenna design, the research group at MDH will use the applicator explained in Chapter 5. The aim is to develop a clinical prototype system for active microwave imaging of the breast and perform trials on patients, and the results from our antenna studies can potentially provide an opening in that direction. At the time of writing the prototype system is being designed and constructed.

The planned mechanical data acquisition system is mainly intended for microwave imaging of the breast but could possibly use other types of sensors for imaging, for example ultrasound and different types of optical sensors. With a change of sensor on the robot arms the hardware system could be customized to fit these imaging technologies as well. This system could also be customized to fit imaging of other parts of the human body. In addition this two arm robot based system should include a vision system to locate the boundaries of the imaging object and from this geometry calculate measurement positions for the two sensors.

Another thinkable feature with the Mamacell system is to include case based reasoning based on Artificial Intelligence (AI). The AI part will calculate the optimum measurement positions in order to completely scan a breast of a certain type (size, density) as well as focusing the imaging attention to a specific domain of the breast. The AI database could be based on comparison measurements with an alternative technique such as MRI or Xray.

Together with some local companies we will develop this measurement equipment called Mamacell. The companies will find new markets, use the developed technology in other projects and create a new products not yet available on the market. The University will be able to continue with successful, innovative research that is usable for industry and the society.

Appendix A

Abbrevations

MWI	Microwave Imaging
RQ	research question
CT	Computed Tomography
MST	Modulated Scattering Technique
MRI	Magnetic Resonance Imaging
MDH	Mälardalen University
VNA	Vector Network Analyzer
PC	polycarbonate
NK	Newton-Kantorovich
MoM	Method of Moments
FEM	Finite Element Method
FDM	Finite Difference method
EFIE	Electrical Field Integral Equation
Q-factor	quality factor
RMS	root mean square
PET	positron emission tomography
NK	Newton-Kantorovich
AI	Artificial Intelligence

Bibliography

[1] Steven P. Poplack, Tor D. Tosteson, Wendy A. Wells, Brian W. Pogue, Paul M. Meaney, Alexander Hartov, Christine A. Kogel, Sandra K. Soho, Jennifer J. Gibson, and Keith D. Paulsen. Electromagnetic Breast Imaging: Results of a Pilot Study in Women with Abnormal Mammograms. *Radiology*, 243(2):350–359, May 2007.

[2] E.C. Fear, J. Bourqui, C. Curtis, D. Mew, B. Docktor, and C. Romano. Microwave breast imaging with a monostatic radar-based system: A study of application to patients. *Microwave Theory and Techniques, IEEE Transactions on*, 61(5):2119–2128, May 2013.

[3] T.M. Grzegorczyk, P.M. Meaney, P.A. Kaufman, R.M. di Florio-Alexander, and K.D. Paulsen. Fast 3-d tomographic microwave imaging for breast cancer detection. *Medical Imaging, IEEE Transactions on*, 31(8):1584–1592, Aug 2012.

[4] M. Klemm, I.J. Craddock, J.A. Leendertz, A. Preece, D.R. Gibbins, M. Shere, and R. Benjamin. Clinical trials of a uwb imaging radar for breast cancer. In *Antennas and Propagation (EuCAP), 2010 Proceedings of the Fourth European Conference on*, pages 1–4, Apr. 2010.

[5] K.L. Carr, P. Cevasco, P. Dunlea, and J. Shaeffer. Radiometric sensing: an adjuvant to mammography to determine breast biopsy. In *Microwave Symposium Digest. 2000 IEEE MTT-S International*, volume 2, pages 929–932 vol.2, June 2000.

[6] A. Fhager, M. Gustafsson, and S. Nordebo. Image reconstruction in microwave tomography using a dielectric debye model. *Biomedical Engineering, IEEE Transactions on*, 59(1):156 –166, Jan. 2012.

[7] T. Rubaek and V. Zhurbenko. Prototype of microwave imaging system for breast-cancer screening. In *Antenna Technology and Applied Electromagnetics and the Canadian Radio Science Meeting, 2009. ANTEM/URSI 2009. 13th International Symposium on*, pages 1–4, Feb 2009.

[8] S.Y. Semenov, A.E. Bulyshev, A. Abubakar, V.G. Posukh, Y.E. Sizov, A.E. Souvorov, P.M. van den Berg, and T.C. Williams. Microwave-tomographic imaging of the high dielectric-contrast objects using different image-reconstruction approaches. *Microwave Theory and Techniques, IEEE Transactions on*, 53(7):2284–2294, July 2005.

[9] Chun Yu, Mengqing Yuan, Yangjun Zhang, J. Stang, R.T. George, G.A. Ybarra, W.T. Joines, and Qing-Huo Liu. Microwave imaging in layered media: 3-d image reconstruction from experimental data. *Antennas and Propagation, IEEE Transactions on*, 58(2):440–448, Feb 2010.

[10] I. Catapano, L. Di Donato, L. Crocco, O. M. Bucci, A. F. Morabito, T. Isernia, and R. Massa. On quantitative microwave tomography of female breast. *Progress In Electromagnetics Research*, 97:75–93, Feb 2009.

[11] M. Ostadrahimi, P. Mojabi, S. Noghanian, L. Shafai, S. Pistorius, and J. LoVetri. A novel microwave tomography system based on the scattering probe technique. *Instrumentation and Measurement, IEEE Transactions on*, 61(2):379–390, Feb 2012.

[12] J. Bourqui, J. M. Sill, and E. C. Fear. A prototype system for measuring microwave frequency reflections from the breast. *Journal of Biomedical Imaging*, 2012:9:9–9:9, January 2012.

[13] M. Klemm, I.J. Craddock, J.A. Leendertz, A. Preece, and R. Benjamin. Radar-based breast cancer detection using a hemispherical antenna array-experimental results. *Antennas and Propagation, IEEE Transactions on*, 57(6):1692 –1704, Jun. 2009.

[14] Xu Li, Essex J. Bond, B.D. Van Veen, and S.C. Hagness. An overview of ultra-wideband microwave imaging via space-time beamforming for early-stage breast-cancer detection. *Antennas and Propagation Magazine, IEEE*, 47(1):19–34, Feb 2005.

[15] Wee Chang Khor, Hua Wang, M.E. Bialkowski, A. Abbosh, and N. Seman. An experimental and theoretical investigation into capabilities of a uwb microwave imaging radar system to detect breast cancer. In *EUROCON, 2007. The International Conference on ;Computer as a Tool*, pages 771 –776, Sept. 2007.

[16] Yao Xie, Bin Guo, Luzhou Xu, Jian Li, and Petre Stoica. Multistatic adaptive microwave imaging for early breast cancer detection. *Biomedical Engineering, IEEE Transactions on*, 53(8):1647–1657, Aug 2006.

[17] Hooi Been Lim, Nguyen Thi Tuyet Nhung, Er-Ping Li, and Nguyen Duc Thang. Confocal microwave imaging for breast cancer detection: Delay-multiply-and-sum image reconstruction algorithm. *Biomedical Engineering, IEEE Transactions on*, 55(6):1697–1704, June 2008.

[18] L.E. Larsen and J.H. Jacobi. Microwave scattering parameter imagery of an isolated canine kidney. *Medical Physics*, 6:394–403, 1979.

[19] J. Jacobi, L.E. Larsen, and C.T. Hast. Water-immersed microwave antennas and their application to microwave interrogation of biological targets. *Microwave Theory and Techniques, IEEE Transactions on*, 27(1):70–78, Jan 1979.

[20] J. Bolomey, A. Izadnegahdar, L. Jofre, Ch Pichot, G. Peronnet, and M. Solaimani. Microwave diffraction tomography for biomedical applications. *Microwave Theory and Techniques, IEEE Transactions on*, 30(11):1998–2000, Nov 1982.

[21] G. Peronnet, Ch Pichot, J. Bolomey, L. Jofre, A. Izadnegahdar, C. Szeles, Y. Michel, J.L. Guerquin-Kern, and M. Gautherie. A microwave diffraction tomography system for biomedical applications. In *Microwave Conference, 1983. 13th European*, pages 529–533, Sept 1983.

[22] J.-C. Bolomey and F.E. Gardiol. *Engineering Applications of the Modulated Scatterer Technique*. Artech House, Aug 2001.

[23] J.-C. Bolomey, L. Jofre, and G. Peronnet. On the possible use of microwave-active imaging for remote thermal sensing. *Microwave Theory and Techniques, IEEE Transactions on*, 31(9):777–781, Sep 1983.

[24] J.M. Rius, C. Pichot, L. Jofre, J.-C. Bolomey, N. Joachimowicz, A. Broquetas, and M. Ferrando. Planar and cylindrical active microwave temperature imaging: numerical simulations. *Medical Imaging, IEEE Transactions on*, 11(4):457–469, Dec 1992.

[25] A. Franchois, A. Joisel, C. Pichot, and J.-C. Bolomey. Quantitative microwave imaging with a 2.45-ghz planar microwave camera. *Medical Imaging, IEEE Transactions on*, 17(4):550–561, Aug 1998.

[26] Alain Joisel and Jean-Charles Bolomey. Rapid microwave imaging of living tissues. In *Proc. of SPIE's International Symposium. Medical Imaging*, volume 3977, pages 320–330, San Diego, CA, USA, Feb 2000.

[27] L. Jofre, M.S. Hawley, A. Broquetas, E. de los Reyes, M. Ferrando, and A.R. Elias-Fuste. Medical imaging with a microwave tomographic scanner. *Biomedical Engineering, IEEE Transactions on*, 37(3):303–312, March 1990.

[28] A. Broquetas, J. Romeu, J.M. Rius, A.R. Elias-Fuste, A. Cardama, and L. Jofre. Cylindrical geometry: a further step in active microwave tomography. *Microwave Theory and Techniques, IEEE Transactions on*, 39(5):836–844, May 1991.

[29] A. Franchois and C. Pichot. Microwave imaging-complex permittivity reconstruction with a levenberg-marquardt method. *Antennas and Propagation, IEEE Transactions on*, 45(2):203–215, Feb 1997.

[30] S.Y. Semenov, R.H. Svenson, A.E. Boulyshev, A.E. Souvorov, V.Y. Borisov, Y. Sizov, A.N. Starostin, K.R. Dezern, G.P. Tatsis, and V.Y. Baranov. Microwave tomography: two-dimensional system for biological imaging. *Biomedical Engineering, IEEE Transactions on*, 43(9):869–877, Sept 1996.

[31] P.M. Meaney, K.D. Paulsen, A. Hartov, and R.K. Crane. An active microwave imaging system for reconstruction of 2-d electrical property distributions. *Biomedical Engineering, IEEE Transactions on*, 42(10):1017–1026, Oct. 1995.

[32] S.Y. Semenov, R.H. Svenson, A.E. Bulyshev, A.E. Souvorov, A.G. Nazarov, Y.E. Sizov, V.G. Posukh, A. Pavlovsky, P.N. Repin, A.N. Starostin, B.A. Voinov, M. Taran, G.P. Tatsis, and V.Y. Baranov. Three-dimensional microwave tomography: initial experimental imaging of animals. *Biomedical Engineering, IEEE Transactions on*, 49(1):55–63, Jan 2002.

[33] M. Klemm, J.A. Leendertz, D. Gibbins, I. J. Craddock, A. Preece, and R. Benjamin. Microwave radar-based breast cancer detection: Imaging in inhomogeneous breast phantoms. *Antennas and Wireless Propagation Letters, IEEE*, 8:1349–1352, 2009.

[34] J.M. Sill and E.C. Fear. Tissue sensing adaptive radar for breast cancer detection - experimental investigation of simple tumor models. *Microwave Theory and Techniques, IEEE Transactions on*, 53(11):3312–3319, Nov 2005.

[35] E.C. Fear, Xu Li, S.C. Hagness, and M.A. Stuchly. Confocal microwave imaging for breast cancer detection: localization of tumors in three dimensions. *Biomedical Engineering, IEEE Transactions on*, 49(8):812–822, Aug 2002.

[36] T. Rubaek, A. Fhager, P.D. Jensen, J.J. Mohr, and M. Persson. Microwave imaging for breast cancer detection: Comparison of tomographic imaging algorithms using single-frequency and time-domain data. In *General Assembly and Scientific Symposium, 2011 XXXth URSI*, pages 1–4, Aug 2011.

[37] M. Miyakawa, T. Ishida, and M. Watanabe. Imaging capability of an early stage breast tumor by cp-mct. In *Engineering in Medicine and Biology Society, 2004. IEMBS '04. 26th Annual International Conference of the IEEE*, volume 1, pages 1427–1430, Sept 2004.

[38] M. Bialkowski, D. Ireland, Yifan Wang, and A. Abbosh. Ultra-wideband array antenna system for breast imaging. In *Microwave Conference Proceedings (APMC), 2010 Asia-Pacific*, pages 267–270, Dec 2010.

[39] M. Jalilvand, C. Wu, J. Schmid, and T. Zwick. Micro detection. *Electronics Letters*, 50(4):238–238, February 2014.

[40] D. Ireland, K. Bialkowski, and A. Abbosh. Microwave imaging for brain stroke detection using born iterative method. *Microwaves, Antennas Propagation, IET*, 7(11):909–915, August 2013.

[41] Mikael Persson, Andreas Fhager, Hana Dobsicek Trefna, Pegah Takook, Yinan Yu, Tomas McKelvey, Jan-Erik Karlsson, Xuezhi Zeng, Herbert Zirath, and Mikael Elam. Microwave based diagnostics and treatment in practice. In *Microwave Workshop Series on RF and Wireless Technologies for Biomedical and Healthcare Applications (IMWS-BIO), 2013 IEEE MTT-S International*, pages 1–3, Dec 2013.

[42] P.M. Meaney, M.W. Fanning, Dun Li, S.P. Poplack, and K.D. Paulsen. A clinical prototype for active microwave imaging of the breast. *Microwave Theory and Techniques, IEEE Transactions on*, 48(11):1841–1853, Nov. 2000.

[43] P.M. Meaney, K.D. Paulsen, and J.T. Chang. Near-field microwave imaging of biologically-based materials using a monopole transceiver system. *Microwave Theory and Techniques, IEEE Transactions on*, 46(1):31–45, Jan 1998.

[44] P.M. Meaney, K.D. Paulsen, J.T. Chang, M.W. Fanning, and Alexander Hartov. Nonactive antenna compensation for fixed-array microwave imaging. ii. imaging results. *Medical Imaging, IEEE Transactions on*, 18(6):508–518, June 1999.

[45] A.H. Golnabi, P.M. Meaney, S. Geimer, and K.D. Paulsen. Microwave imaging for breast cancer detection and therapy monitoring. In *Biomedical Wireless Technologies, Networks, and Sensing Systems (BioWireleSS), 2011 IEEE Topical Conference on*, pages 59–62, Jan 2011.

[46] A.H. Golnabi, P.M. Meaney, and K.D. Paulsen. Tomographic microwave imaging with incorporated prior spatial information. *Microwave Theory and Techniques, IEEE Transactions on*, 61(5):2129–2136, May 2013.

[47] A.H. Golnabi, P.M. Meaney, S. Geimer, Tian Zhou, and K.D. Paulsen. Microwave tomography for bone imaging. In *Biomedical Imaging: From Nano to Macro, 2011 IEEE International Symposium on*, pages 956–959, March 2011.

[48] P.M. Meaney, D. Goodwin, A.H. Golnabi, Tian Zhou, M. Pallone, S.D. Geimer, G. Burke, and K.D. Paulsen. Clinical microwave tomographic imaging of the calcaneus: A first-in-human case study of two subjects. *Biomedical Engineering, IEEE Transactions on*, 59(12):3304–3313, Dec 2012.

[49] T. Henriksson, M. Klemm, D. Gibbins, J. Leendertz, T. Horseman, A.W. Preece, R. Benjamin, and I.J. Craddock. Clinical trials of a multistatic uwb radar for breast imaging. In *Antennas and Propagation Conference (LAPC), 2011 Loughborough*, pages 1–4, Nov 2011.

[50] P.M. Meaney, D. Goodwin, A. Golnabi, M. Pallone, S. Geimer, and K.D. Paulsen. 3d microwave bone imaging. In *Antennas and Propagation (EUCAP), 2012 6th European Conference on*, pages 1770–1771, March 2012.

[51] C. Pichot, L. Jofre, G. Peronnet, and J.-C. Bolomey. Active microwave imaging of inhomogeneous bodies. *Antennas and Propagation, IEEE Transactions on*, 33(4):416–425, Apr 1985.

[52] Frank J. Paoloni. The effects of attenuation on the born reconstruction procedure for microwave diffraction tomography (short paper). *Microwave Theory and Techniques, IEEE Transactions on*, 34(3):366–368, Mar 1986.

[53] M. Slaney, A.C. Kak, and L.E. Larsen. Limitations of imaging with first-order diffraction tomography. *Microwave Theory and Techniques, IEEE Transactions on*, 32(8):860–874, Aug 1984.

[54] E. Salerno. Microwave tomography of lossy objects from monostatic measurements. *Microwave Theory and Techniques, IEEE Transactions on*, 47(7):986–994, Jul 1999.

[55] N. Joachimowicz, C. Pichot, and J.-P. Hugonin. Inverse scattering: an iterative numerical method for electromagnetic imaging. *Antennas and Propagation, IEEE Transactions on*, 39(12):1742–1753, Dec 1991.

[56] S. Caorsi, G.L. Gragnani, and M. Pastorino. Two-dimensional microwave imaging by a numerical inverse scattering solution. *Microwave Theory and Techniques, IEEE Transactions on*, 38(8):981–989, Aug 1990.

[57] P.M. Meaney, K.D. Paulsen, and T.P. Ryan. Two-dimensional hybrid element image reconstruction for tm illumination. *Antennas and Propagation, IEEE Transactions on*, 43(3):239–247, Mar 1995.

[58] T. Henriksson, N. Joachimowicz, C. Conessa, and J.-C. Bolomey. Quantitative microwave imaging for breast cancer detection using a planar 2.45 ghz system. *Instrumentation and Measurement, IEEE Transactions on*, 59(10):2691–2699, Oct. 2010.

[59] T. Henriksson. *Contribution to Quantitative Microwave Imaging Techniques for Biomedical Applications*. PhD thesis, Mälardalen University, Press Dissertation, Jun. 2009.

[60] P.M. Meaney, N.K. Yagnamurthy, Dun Li, E. Demidenko, and K.D. Paulsen. A 2-stage gauss-newton reconstruction technique for improved object detection in microwave imaging. In *Antennas and Propagation Society International Symposium, 2001. IEEE*, volume 1, pages 238–241 vol.1, July 2001.

[61] J. De Zaeytijd, A. Franchois, C. Eyraud, and J. M Geffrin. Full-wave three-dimensional microwave imaging with a regularized gauss newton method - theory and experiment. *Antennas and Propagation, IEEE Transactions on*, 55(11):3279–3292, Nov 2007.

[62] A. Fhager and M. Persson. Using a priori data to improve the reconstruction of small objects in microwave tomography. *Microwave Theory and Techniques, IEEE Transactions on*, 55(11):2454–2462, Nov 2007.

[63] S. Caorsi, E. Bermani, and A. Massa. A finite-element procedure based on a boundary-value approach for the evaluation of the electromagnetic exposure in biological phantoms. *Microwave Theory and Techniques, IEEE Transactions on*, 50(10):2346–2352, Oct 2002.

[64] S.Y. Semenov, A.E. Bulyshev, A. Abubakar, V.G. Posukh, Y.E. Sizov, A.E. Souvorov, P.M. van den Berg, and T.C. Williams.

Microwave-tomographic imaging of the high dielectric-contrast objects using different image-reconstruction approaches. *Microwave Theory and Techniques, IEEE Transactions on*, 53(7):2284–2294, July 2005.

[65] A. Abubakar, S. Semenov, V.G. Posukh, and P.M. van den Berg. Application of the multiplicative regularized contrast source inversion method to real biological data. In *Microwave Symposium Digest, 2005 IEEE MTT-S International*, pages 4 pp.–, June 2005.

[66] A. Abubakar, T.M. Habashy, Guangdong Pan, and Mao-Kun Li. Application of the multiplicative regularized gauss newton algorithm for three-dimensional microwave imaging. *Antennas and Propagation, IEEE Transactions on*, 60(5):2431–2441, May 2012.

[67] M. Ostadrahimi, P. Mojabi, A. Zakaria, J. LoVetri, and L. Shafai. Enhancement of gauss newton inversion method for biological tissue imaging. *Microwave Theory and Techniques, IEEE Transactions on*, 61(9):3424–3434, Sept 2013.

[68] M. Klemm, I. J. Craddock, J. A. Leendertz, A. Preece, and R. Benjamin. Improved delay-and-sum beamforming algorithm for breast cancer detection. *International Journal of Antennas and Propagation*, 2008.

[69] M. Klemm, J.A. Leendertz, D. Gibbins, I.J. Craddock, A. Preece, and R. Benjamin. Microwave radar-based differential breast cancer imaging: Imaging in homogeneous breast phantoms and low contrast scenarios. *Antennas and Propagation, IEEE Transactions on*, 58(7):2337 –2344, Jul. 2010.

[70] Hooi Been Lim, Nguyen Thi Tuyet Nhung, Er-Ping Li, and Nguyen Duc Thang. Confocal microwave imaging for breast cancer detection: Delay-multiply-and-sum image reconstruction algorithm. *Biomedical Engineering, IEEE Transactions on*, 55(6):1697–1704, June 2008.

[71] Xu Li, Essex J. Bond, B.D. Van Veen, and S.C. Hagness. An overview of ultra-wideband microwave imaging via space-time beamforming for early-stage breast-cancer detection. *Antennas and Propagation Magazine, IEEE*, 47(1):19–34, Feb 2005.

[72] Wee Chang Khor, Hua Wang, M.E. Bialkowski, A. Abbosh, and N. Seman. An experimental and theoretical investigation into capabilities of a uwb microwave imaging radar system to detect breast cancer. In *EUROCON, 2007. The International Conference on Computer as a Tool*, pages 771–776, Sept 2007.

[73] Government Health Sweden (Socialstyrelsen). Cancer incidence in Sweden in 2012. New cancer cases diagnosed in 2012. `http://www.socialstyrelsen.se/Lists/Artikelkatalog/Attachments/19291/2013-12-17.pdf`, 2014. [Online; accessed 6-February-2014].

[74] J. Ferlay, I. Soerjomataram, M. Ervik, R. Dikshit, S. Eser, C. Mathers, M. Rebelo, D.M. Parkin, D. Forman, and F. Bray. GLOBOCAN 2012 v1.0, Cancer Incidence and Mortality Worldwide: IARC CancerBase No. 11. Lyon, France: International Agency for Research on Cancer; 2013. `http://globocan.iarc.fr`. [Online; accessed 6-February-2014].

[75] Cancerfonden. Mammografi. `http://www.cancerfonden.se/sv/cancer/Forebygga-och-risker/Tidig-upptackt/Mammografi/`, 2014. [Online; accessed 6-February-2014].

[76] J.S. Nass, I.C. Henderson, and J.C. Lasho. *Mammography and Beyond: Developing Technologies for the Early Detection of Breast Cancer*. National Academy of Sciences, Aug 2001.

[77] W.C. Chew and Y.M. Wang. Reconstruction of two-dimensional permittivity distribution using the distorted born iterative method. *Medical Imaging, IEEE Transactions on*, 9(2):218–225, Jun 1990.

[78] A. Franchois and C. Pichot. Microwave imaging-complex permittivity reconstruction with a levenberg-marquardt method. *Antennas and Propagation, IEEE Transactions on*, 45(2):203–215, Feb 1997.

[79] N. Joachimowicz, J.J. Mallorqui, J. C Bolomey, and A. Broquets. Convergence and stability assessment of newton-kantorovich reconstruction algorithms for microwave tomography. *Medical Imaging, IEEE Transactions on*, 17(4):562–570, Aug. 1998.

[80] P.M. Meaney, M.W. Fanning, S.D. Geimer, and K.D. Paulsen. Mutual coupling in a tomographic imaging system. In *Antennas and Propagation, 2009. EuCAP 2009. 3rd European Conference on*, pages 2948–2949, Mar.

[81] M. Lazebnik, L. McCartney, D. Popovic, C.B. Watkins, M.J. Lindstrom, J. Harter, S. Sewall, A. Magliocco, J.H. Booske, M. Okoniewsk, and S.C. Hagness. A large-scale study of the ultrawideband microwave dielectric properties of normal breast tissue obtained from reduction surgeries. *Phys. Med. Biol*, 52(10):2637–2656, May 2007.

[82] M. Lazebnik, D. Popovic, L. McCartney, C.B. Watkins, M.J. Lindstrom, J. Harter, S. Sewall, T. Ogilvie, A. Magliocco, T. M. Breslin, W. Temple, D. Mew, J.H. Booske, M. Okoniewsk, and S.C. Hagness. A large-scale study of the ultrawideband microwave dielectric properties of normal, benign and malignant breast tissues obtained from cancer surgeries. *Phys. Med. Biol*, 52(20):6093–6115, Oct. 2007.

[83] William T. Joines, Randy L. Jirtle, Marc D. Rafal, and Daniel J. Schaefer. Microwave power absorption differences between normal and malignant tissue. *International Journal of Radiation Oncology*Biology*Physics*, 6(6):681 – 687, 1980.

[84] William T. Joines, Yang Zhang, Chenxing Li, and Randy L. Jirtle. The measured electrical properties of normal and malignant human tissues from 50 to 900 mhz. *Medical Physics*, 21(4):547–550, 1994.

[85] S.S. Chaudhary, R.K. Mishra, A. Swarup, and J.M. Thomas. Dielectric properties of normal and malignant human breast tissues at radiowave and microwave frequencies. *Medical Physics*, 21:76–79, 1984.

[86] A.J. Surowiec, S.S. Stuchly, J.R. Barr, and A. Swarup. Dielectric properties of breast carcinoma and the surrounding tissues. *Biomedical Engineering, IEEE Transactions on*, 35(4):257–263, April 1988.

[87] Jyh Sheen. Study of microwave dielectric properties measurements by various resonance techniques. *Measurement*, 37(2):123 – 130, 2005.

[88] P.M. Meaney, K.D. Paulsen, and J.T. Chang. Near-field microwave imaging of biologically-based materials using a monopole transceiver system. *Microwave Theory and Techniques, IEEE Transactions on*, 46(1):31 –45, Jan. 1998.

[89] A. Stogryn. Equations for calculating the dielectric constant of saline water (correspondence). *Microwave Theory and Techniques, IEEE Transactions on*, 19(8):733–736, Aug. 1971.

[90] A.J. Surowiec, S.S. Stuchly, J.R. Barr, and A. Swarup. Dielectric properties of breast carcinoma and the surrounding tissues. *Biomedical Engineering, IEEE Transactions on*, 35(4):257 –263, Apr. 1988.

[91] Xu Li, S.K. Davis, S.C. Hagness, D.W. van der Weide, and B.D. Van Veen. Microwave imaging via space-time beamforming: experimental investigation of tumor detection in multilayer breast phantoms. *Microwave Theory and Techniques, IEEE Transactions on*, 52(8):1856–1865, Aug. 2004.

[92] M. Jalilvand, X. Li, J. Kowalewski, and T. Zwick. Broadband miniaturised bow-tie antenna for 3d microwave tomography. *Electronics Letters*, 50(4):244–246, February 2014.

[93] Reza K. Amineh, M. Ravan, A. Trehan, and N.K. Nikolova. Near-field microwave imaging based on aperture raster scanning with tem horn antennas. *Antennas and Propagation, IEEE Transactions on*, 59(3):928–940, March 2011.

[94] Jingjing Zhang, Elise C. Fear, and Ronald H. Johnston. Cross-vivaldi antenna for breast tumor detection. *Microwave and Optical Technology Letters*, 51(2):275–280, 2009.

[95] J. Bourqui, M. Okoniewski, and E.C. Fear. Balanced antipodal vivaldi antenna for breast cancer detection. In *Antennas and Propagation, 2007. EuCAP 2007. The Second European Conference on*, pages 1–5, Nov 2007.

[96] J. Bourqui, M. Okoniewski, and E.C. Fear. Balanced antipodal vivaldi antenna with dielectric director for near-field microwave imaging. *Antennas and Propagation, IEEE Transactions on*, 58(7):2318–2326, July 2010.

[97] D. Gibbins, M. Klemm, I.J. Craddock, J.A. Leendertz, A. Preece, and R. Benjamin. A comparison of a wide-slot and a stacked patch antenna for the purpose of breast cancer detection. *Antennas and Propagation, IEEE Transactions on*, 58(3):665–674, March 2010.

[98] J. Bourqui and E.C. Fear. Shielded uwb sensor for biomedical applications. *Antennas and Wireless Propagation Letters, IEEE*, 11:1614–1617, 2012.

[99] J. Bourqui and E.C. Fear. Systems for ultra-wideband microwave sensing and imaging of biological tissues. In *Antennas and Propagation (EuCAP), 2013 7th European Conference on*, pages 834–835, April 2013.

[100] Jeremie Bourqui. Eccostock breast model. Internal report, University of Calgary, April 2012.